Coordination Chemistry Reviews 441 (2021) 213977

Contents lists available at ScienceDirect

Coordination Chemistry Reviews

journal homepage: www.elsevier.com/locate/ccr

Review

Antitumour activity of coordination polymer nanoparticles

Salvio Suárez-García [a], Rubén Solórzano [a,b], Ramon Alibés [b], Félix Busqué [b], Fernando Novio [b,*], Daniel Ruiz-Molina [a,*]

[a] Catalan Institute of Nanoscience and Nanotechnology (ICN2), CSIC and BIST, Campus UAB, Bellaterra, 08193 Barcelona, Spain
[b] Departament de Química, Universitat Autònoma de Barcelona (UAB), Campus UAB, Cerdanyola del Vallès, 08193 Barcelona, Spain

ARTICLE INFO

Article history:
Received 28 December 2020
Accepted 11 April 2021
Available online 8 May 2021

Keywords:
Multifunctional nanoparticle
Coordination polymer
Theranostic
Cancer therapy

ABSTRACT

Nanoscale coordination polymers (NCPs) have fascinated researchers over the last years. Their intrinsic theranostic properties of metal ions and organic ligands, the encapsulation of several drugs/biomolecules with excellent yields and the surface functionalisation, enhancing their biocompatibility and targeting, have remarkably impacted in prospective drug delivery alternatives in medicine. Moreover, the properties and characteristics of these nanoparticles (NPs) can be fine-tuned thanks to the synthetic flexibility of coordination chemistry. For all these reasons, the number of examples published has grown exponentially over the last years, embracing different disciplines such as molecular electronics, sensors or nanomedicine, among others. Specifically, significant advances in antitumoural applications are reported, one of the areas where this novel family of NPs has experienced a considerable advance. NCPs have accomplished a high sophistication degree and efficiency as theranostic nanoplatforms (i.e., drug delivery carriers and bioimaging probes) with long residence time in the bloodstream, targeting capacities and remarkable cellular internalisation. In this review, an introduction emphasizing the advantages of NPs for cancer treatment is included. Later on, the most representative examples of NCPs for antitumoural applications are described grouped into six mean representative areas: i) encapsulation approaches, ii) stimuli-responsive NCPs, iii) metal chemotherapy, iv) photodynamic therapy (PDT), v) unconventional therapeutic approaches and vi) theranostics. Particular emphasis is given to understand the encapsulation/release properties of these particles at the nanoscale and their interaction with biological environments, highlighting any limitation and challenges that these systems are facing from a clinical translation perspective and envisioning possible future trends and areas that will deserve further attention for the following years.

Contents

* Corresponding authors.
E-mail addresses: fernando.novio@uab.cat (F. Novio), dani.ruiz@icn2.cat (D. Ruiz-Molina).

https://doi.org/10.1016/j.ccr.2021.213977
0010-8545/

1. Introduction

The incorporation of nanoparticles (NPs) for antitumoral treatment dates back to 1986, with the first evidence for their accumulation into tumoural areas due to enhanced permeation and retention (EPR) effect. Due to their fast and uncontrolled growth, tumoural cells generate poorly formed blood vessels with defects hundred nanometers in size that ensure significant contributions of nutrients and oxygen (difficult to achieve with conventional blood vessels, especially for large tumours). Those are the same holes that facilitate the access of the NPs to the tumoural tissue [1], which once inside are consistently retained [2]. Other advantages for the use of NPs as drug carriers are: i) improvement of the drug pharmacokinetic profile, ii) enhanced chemical protection, iii) use of lipophilic drugs, iv) increase of the circulation time concerning the free drug, and v) diminish prescriptions thus less toxicity [3]. Thanks to all these benefits, exponentially increasing examples of nanoplatforms for antitumoural applications have been reported over the years, reaching in some specific cases the market [4]. Among them, the Food and Drug Administration (FDA) has approved liposomes (35%) and nanocrystals (25%), emulsions (15%), iron-based polymer complexes (10%), micelles (5%), or other nanosystems (15%) [5]. Overall, nanomedicine stands nowadays for more than 22% of all commercial drugs and continuously rising every day [6], from where oncology represents almost 35% [7]. Since 1995, around 50 nano-based pharmaceuticals have been authorised by the FDA and are presently accessible for clinical assays, and more than 60 are under clinical evaluation [8].

Beyond the examples of nanocarriers previously described, several other families of NPs have also been described in the literature. Most of them are polymeric NPs and liposomes [9] or inorganic systems such as metallic or ceramic NPs [10–12]. Worth emphasizing, porous NPs have high payloads, low toxicity, chemical robustness and scalable production [13]. For instance, mesoporous silica NPs (MSNs) with high empty volume and pore size between 2 and 5 nm allows for high loading capacities and surface functionalisation (both internal and external) with different molecules and biomolecules through one-pot reaction or after particle formation (post-synthesis) [14]. An alternative family of porous nanocarriers attracting growing interest is nanoscale metal–organic frameworks (NMOFs) [15]. Thanks to the wealth and synthetic flexibility of coordination chemistry, NMOFs can be

Abbreviations: AA, anisamide; ADME, absorption, distribution, metabolism, and excretion; AIE, aggregation-induced emission enhancement; ALN, alendronate; AsPC-1, pancreatic cancer cell line; AZT, azidothymidine; A431, epidermoid carcinoma; BATA, bis–(alkylthio) alkene linker; BPEI, branched polyethyleneimine; BSA, Bovine Serum Albumin; BTB, 4,4′,4″-benzene-1,3,5-triyl-tri-benzoic acid; CA, contrast agent; CBTA, cyclobutane-1,2,3,4-tetracarboxylic dianhydride; Ce6, chlorine e6; CD44+, CD44 overexpressing cancer cell line; CD44-, CD44 minimal-expressing cell line; CHG, S-(N-p-chlorophenyl- N-hydroxycarbamoyl)glutathione; CLSM, confocal laser scanning microscopy; CP, coordination polymer; CpG, cytosine triphosphate deoxynucleotide linked to guanine triphosphate deoxynucleotide ; NCP, coordination polymer nanoparticle; CPT, camptothecin; CT, computed tomography; CT-DNA, calf thymus DNA; CT26, colon cancer cell line; DAU, daunomycin; DHA, dihydroartemesinin; DLS, dynamic light scattering; DMCA, dual-mode contrast agent; DNA, deoxyribonucleic acid; DNP, dipeptide NPs; DOX, doxorubicin; dpac, dipyrido[3,2-a:2′,3′-c](6,7,8,9-tetrahydro)phenazine; dpg, dipyrido[3,2-d:2′,3′-f]quinoxaline; DPN, dip-pen nanolithography; DSP, c,c,t-(diamminedichlorodisuccinato)Pt(IV); Fc, 1,1′-dicarboxyl ferrocene, FDA, U.S. Food and Drug Administration; EPR, enhanced permeability and retention effect; ECM, tumour extracellular matrix; EDA, ethylenediamine; EGCG, epigallocatechin-3-gallate; GA, gallic acid; GcMP, gemcitabine monophosphate; GMP, guanosin monophosphate; GSH, glutathione; GT, genetherapy; HOPO, 3-hydroxy-4-pyridinone; HCT116, human colorectal cells; HeLa, cervical cancer cells; Hemin, Fe-containing porphyrin; Hep-2, laryngeal cancer cell line; Hep G2, human liver cancer cell line; HT29, human colon cancer cell line; HmA, hexahistidine-metal nanoassemblies; H460, lung cancer cell line; ICG, indocyanine green; IC_{50}, half maximal inhibitory concentration; ip, imidazo [4,5-f]1,10-phenanthroline; i.v., intravenous; MCF-7, human breast adenocarcinoma cells; MDR, multidrug resistant; miRNA, micro ribonucleic acid; MRI, magnetic resonance imaging; MSNs, mesoporous silica NPs; MTX, methotrexate; N-BP, Nitrogen containing bisphosphonates; NCI-H446/60, human lung cancer cells; NIR, near-infrared; NMOF, nanoscale metal–organic framework; NP, nanoparticle; OCa, ovarian cancer; OxPt, oxaliplatin; PA, piperazine; PAI, photoacoustic imaging; PAT, photoacoustic tomography; PDA, polydopamine; PDT, photodynamic therapy; PEG, polyethylene glycol; PEGMA, mPEG-grafted poly(methacrylate); PEG-PBHE-PS, poly(ethylene glycol)-b-poly(2-hydroxyethyl methacrylate-Boc-histidine)-b-poly(styrene); PEO, poly(ethylene-oxide); PET, positron emission tomography; pHis-PEG, poly-L-histidine-PEG; PPT, photothermal therapy; PVP, polyvinylpyrrolidone; QD, quantum dot; rhod, rhodamine; RI, radioimaging; RGD, arginylglycylaspartic acid; RNA, ribonucleic acid; ROX, reactive oxygen species; r_1, longitudinal relaxation value; r_2, transversal relaxation value; SEM, scanning electron microscopy; siRNA, small interfering ribonucleic acid; SKOV-3, ovarian cancer cell line; SPECT, single-photon emission computed–tomography; SPIONs, superparamagnetic iron oxide NPs; TA, tannic acid; TCPP, meso-tetrakis(4-carboxyl)-21H,23H-porphirine; TNTs, titania nanotubes; TPPGC, chloro(triphenylphosphine)gold(I); TPZnPc, tetra(4-carboxyphenoxy)-phthalocyaninatozinc(II); T_1, longitudinal relaxivity; T_2, transversal relaxivity; T_{1w}, T_1 weighted imaging contrast; T_{2w}, T_2 weighted imaging contrast; ZnPc, zinc phthalocyanine, 4T1, breast cancer cell line

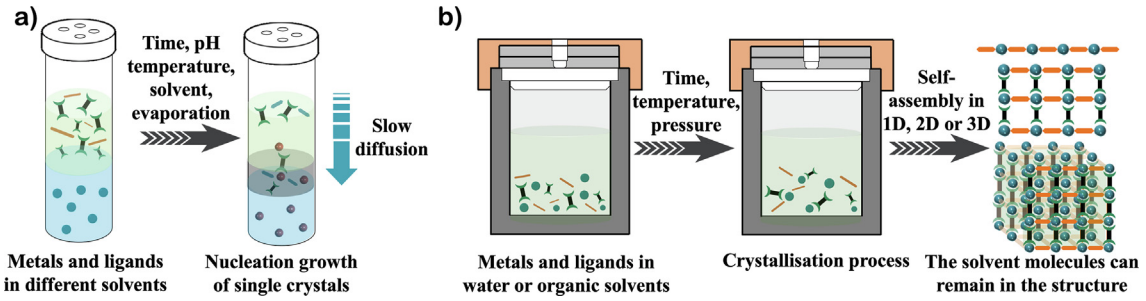

Fig. 1. Main synthetic methodologies for the synthesis of porous and crystalline metal–organic frameworks (MOFs). a) the controlled diffusion of the separated components into the selected solvents with different densities leads to slowing the coordination reaction speed. The diffusion–reaction becomes useful for growing good-shaped and good-quality single crystals; b) hydro-/solvothermal approach to form 1D, 2D, and 3D coordination polymers (CPs). The precursors are added and mixed in a specific solvent within a sealed container. The application of temperature leads to reach the suitable conditions for the formation of crystals after a given period.

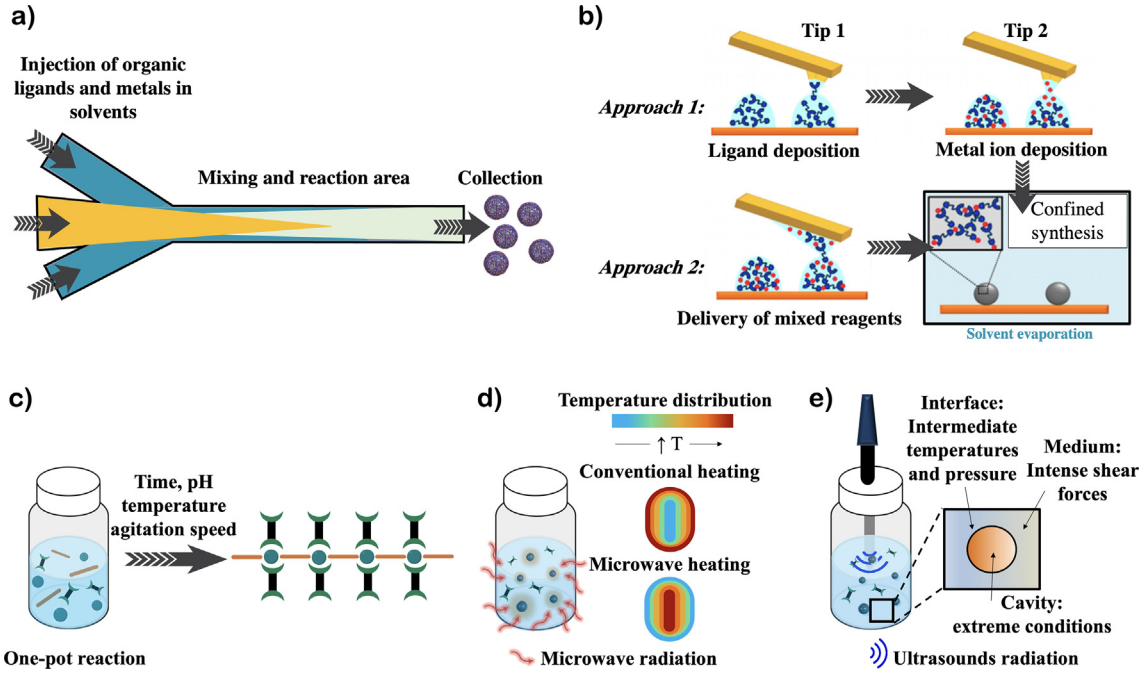

Fig. 2. Main synthetic methodologies used for the synthesis of nanoscale coordination polymers (NCPs). a) lab-on-a-chip device where the starting materials are injected into the inlet and slowly diffuse to the mixing and reaction area, yielding the final product that is collected at the end of the device; b) use of atomic force microscopy (AFM) nanolithography (Dip-Pen) for the direct synthesis of NCPs on surfaces using femtolitre droplets, both mixing the reactant directly on the surface or previously in the ink holder; c) one-pot synthesis reaction; d) and assisted with microwave radiation that locally increase the temperature with low dissipation; e) the energy received from ultrasound radiation allows for acoustic cavitation formation that generates a localised increase in temperature and pressure. The figure shown in panel b is adapted from Ref. [25] with permission of the copyright holder.

obtained with different geometries, dimensions, functionalities and exceptionally high loadings thanks to their remarkable porosity (from 1000 up to 10,000 m^2/g) [16]. Beyond encapsulation within the pores, it is also possible to attach the drug to the constitutive metal ions of the polymeric network [17–20], which in turn may be simultaneously used as contrast agents (CAs) [21]. There are specific synthetic strategies to control the crystallinity and porosity of the final products, usually using methods that accurately control some parameters such as diffusion (Fig. 1**a**) or pressure and temperature (solvothermal) (Fig. 1**b**).

Alternatively to NMOFs, nanoscale coordination polymers (NCPs) have also raised increasing interest since first reported by Mirkin [22] and Wang [23] back in 2005. Various approaches have been used for their synthesis, ranging from the use of sophisticated lab-on-a-chip devices [24] (Fig. 2**a**) or Dip-Pen Nanolithography (DPN) [25,26] (Fig. 2**b**) to other methods [27] as reverse microemulsions [28]. However, the most shared and simple approach is the synthesis of the NPs using out-of-equilibrium conditions, mainly by a one-pot reaction of organic ligands, metal ions and a co-solvent that promotes a fast precipitation (Fig. 2**c**), a process that can be assisted by external stimuli such as microwave (Fig. 2**d**) or ultrasounds (Fig. 2**e**) [176].

The resulting NPs are usually amorphous and less porous than NMOFs, with a spherical shape to lessen the interfacial free energy and average dimensions regulated by the addition rate of the co-solvent [29]. Moreover, the synthesis is fully reproducible and scalable, in addition, to exhibit the following characteristics: i) excellent colloidal stabilities, ii) multifunctional properties [30], iii) encapsulation of several drugs with excellent yields and control release, and iv) control of the surface functionality, improving their biocompatible character (Fig. 3**c**) [31,32]. A representative example compiling most of such potentialities was given by Novio *et col.*, who reported NCPs containing carboxyl ended ligands favouring improved thermal and colloidal stabilities (Fig. 3**a**). Moreover, surface carboxyl groups were functionalised with different functional groups through well-known

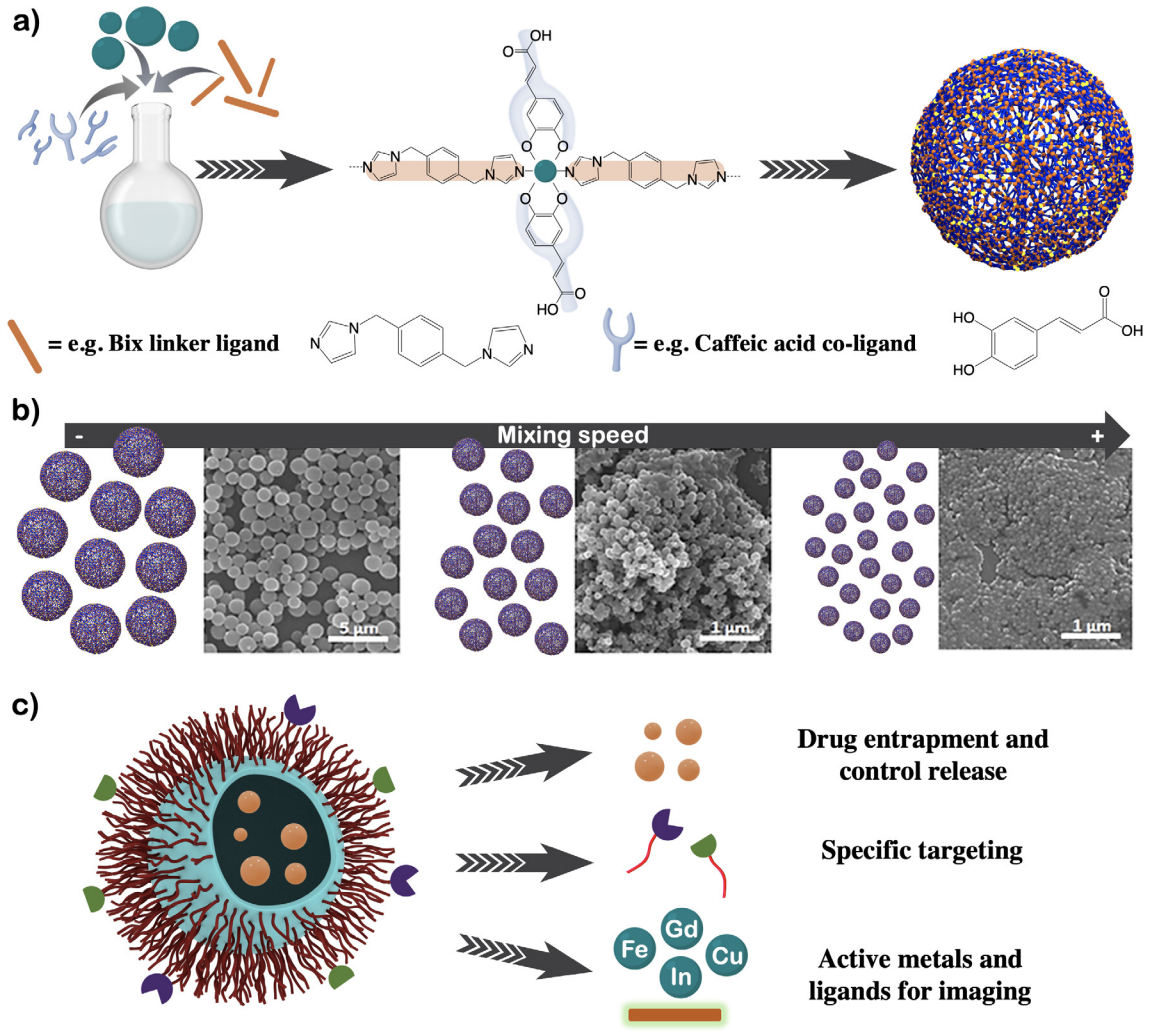

Fig. 3. a) representative out-of-equilibrium synthesis of NCPs using caffeic acid, bis-imidazol linker (1,4-Bis(imidazol-1-ylmethyl)benzene) (Bix) ligands and a metal salt; b) scanning electron microscopy (SEM) images showing different synthetic batches of nanoparticles (NPs) with tuned dimensions by controlling the reaction mixing speed; c) schematic representation of NCPs advantages: feasibility to incorporate different surface functionalities to favour their colloidal stability, signalling and targeting abilities, drug entrapment, and control release, imaging, biocompatibility or their integration into more complex hybrid systems. SEM images are reproduced from Ref. [33] with permission of the copyright holder.

peptide coupling reactions [33]. This strategy endowed enhanced biocompatibility and colloidal stability [34] or hybrid composites formation [35]. All of this is favoured by the attachment of specific molecules on the particle surface (i.e., peptides, antibodies, or aptamers, among others), increasing the active targeting to cancer tissues [36].

Concerning the area of application, NCPs have become relevant in different fields such as gas adsorption and separation processes [37], catalysis [38], sensor devices [39], photoluminescence [40], energy harvesting and conductivity [41]. Each one of these applications requires specific characteristics and stabilities though that of nanomedicine is probably one of the most restrictive. For the succesful application in this area, NCPs must fulfill specific needs that are listed next:

i) *Size*. The final diameter of the NCPs must be in the nm range. The size will influence the biodistribution and clearance of the developed systems. Smaller NPs (<20 nm) can be easily and quickly cleaned from the body, while bigger NPs (>100 nm) can be retained for longer circulation times. The required sizes will depend on the administration route and also on the final target tissue. For example, reaching the brain through intravenous (i.v.) injection requires crossing the blood–brain barrier. In this case, small NPs must be used. Nevertheless, if the NPs are administered intranasally, the sizes can be larger.

ii) *Colloidal stability*. NCPs must demonstrate excellent colloidal stability in water and physiological conditions. Colloidal dispersions of NCPs have to be achieved, thus avoiding aggregation and agglomeration processes, which will hamper their final application. This colloidal stability have to be long enough to ensure the performance of the NCPs.

iii) *Biocompatibility and biodegradability*. The biocompatibility will be directly related to the metals and organic ligands employed NCPs and must be tested in healthy tissues to ensure their safety. To reduce potential side effects, a careful predesign should be considered. How the NCPs decompose will significantly affect their potential use in biomedicine. For example, the leaching of harmful metals can induce their accumulation in some organs causing pathologies in the medium-long term. The biodegradability of the NCPs is also of vital importance and all the species from the NCP decomposition must be safe and adequately metabolised/cleared by the organism.

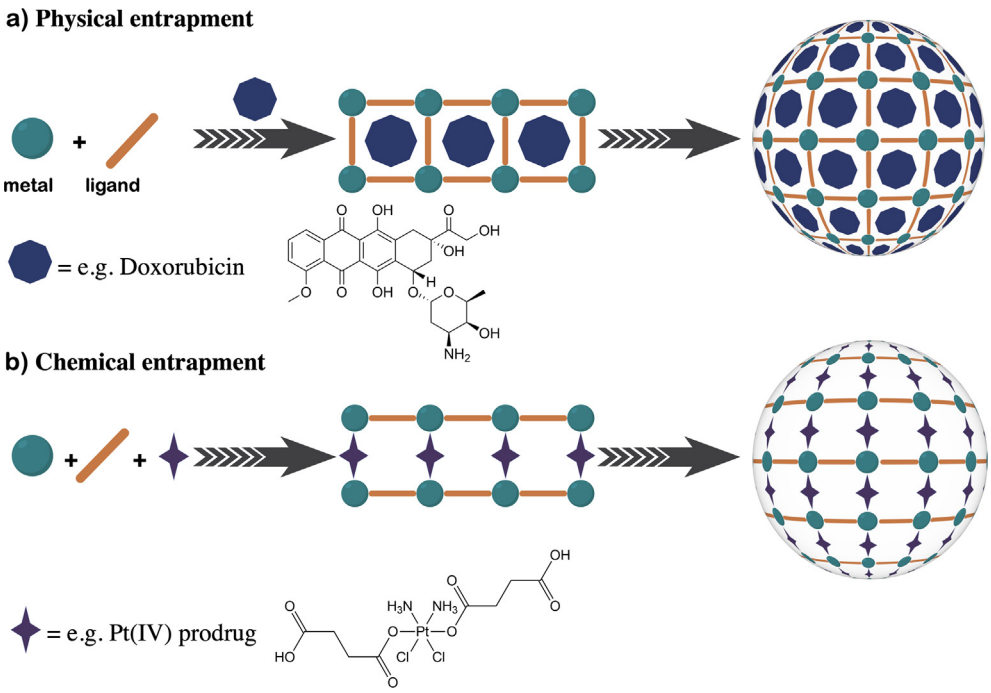

Fig. 4. Representation of the two approaches used to encapsulate active drugs in NCPs: a) physical entrapment; b) chemical entrapment.

iv) *Shape and robustness.* The most frequent round shaped morphology of NCPs facilitates its circulation through the bloodstream and properly biodistribution in the whole organism. What is even more important is the robustness of the NCPs. The degree of rigidity/softness will facilitate its internalization through the organism and its final clearance.

v) *Functionalisation.* The presence of ready-to-use functional groups as anchoring points on the surface of NCPs turns out to be very useful. In most cases, the NCPs are not intrinsically tumour-selective, and the EPR effect is not enough to ensure its effective accumulation in the tumoural area. To avoid harmful effects in healthy tissues, the surface of NCPs must be decorated with specific moieties (e.g., antibodies, peptides and active pharmacological molecules, among others), ensuring its selective recognition and locally limiting its effect. Other functionalities can be added to improve the properties of the developed NCPs, such as biocompatibility and colloidal stability (e.g., PEGylation or protein corona formation).

2. Encapsulation approaches in NCPs

Encapsulation within NCPs takes place mostly through two different strategies (or a combination of both), which are schematically depicted in Fig. 4. In the first of the approaches (physical entrapment), encapsulation inside the nanostructure occurs along the particle assembly modulated by the chemical nature of the metals and ligands [42]. The second approach (chemical entrapment) consists in the incorporation of the active drug or imaging probe as a constitutive building block of the NCP [43]. This can be achieved using two different methodologies: i) incorporation of bio-active metal ions as connecting building blocks (e.g., Fe, Zn, Mn, Ag, Gd) or ii) incorporation of drugs as organic ligands. Consequently, the drug release in both entrapment approaches occurs through different pathways: i) NP disintegration due to its surface degradation, ii) diffusion of the active drugs through the polymeric matrix, or iii) a combination of both [44]. Both approaches are explained in more detail next.

2.1. Physical entrapment

The physical entrapment of organic/inorganic luminescent dyes and magnetic NPs with good encapsulation yields was already reported back in 2009 [42]. The same authors also showed how NCPs could encapsulate anticancer drugs with efficiencies up to 21%, released with time [45]. In another work, Gao *et col.* reported Fe-based NCPs coated with silica to increase their stability in physiological environments, allowing for a sustained drug release of several days in response to slight pH modifications [46]. Moreover, functionalisation of the silica with folic acid provided the NPs with targeting properties against cancer cells. Liang *et col.* also reported triblock copolymer nanowires bearing a complex of β-cyclodextrin, and 4,4′-bipyridine in the presence of Ni(II), which incorporated the Nile red dye as organic cargo [47]. Recent designs furthermore included nanogels containing doxorubicin (Dox) obtained upon coordination of Fe(III) with dopamine-base gelatin polymeric materials [48]. These novel nanogels exhibited excellent cytocompatibility and efficient penetration into the cell membrane. Interestingly, this nanoformulation showed a delayed drug efficacy in comparison to free Dox.

2.2. Chemical entrapment

As commented before, an alternative approximation to physical entrapment consists in the direct incorporation of active drugs (metal ions or organic ligands) as constitutive units of the polymeric backbone with smart release responses in front of external stimuli (e.g., pH, enzymatic action, a reducing environment or light). In this sense, Xing *et col.* reported the formation of different NPs combining methotrexate (MTX) and S-(N-p-chlorophenyl-N-hydroxycarbamoyl)glutathione (CHG, the human glyoxalase I inhibitor) with Zn or Fe ions. The stabilisation of the NPs was achieved by coating with another coordination polymer (CP) layer made of Zn ions and 1,4-bis(imidazol-1-ylmethyl)benzene (bix) [49], silica, or a lipid bilayer [50]. The differential robustness and degradation of the coatings were used to fine-tune the drug release profile in front of varying physiological conditions. Later on, Yan *et col.*

demonstrated the formation of curcumin- and Zn(II)-based NCPs with preferential accumulation in tumours and controlled degradation in physiological environments [51]. Li *et col.* reported Fe-induced DNA self-assemblies with tunable Fe:nucleotide ratios [52]. These systems were efficiently uptaken by the cells, showing a predominant presence in endosomes or lysosomes. Besides, DNA delivery was possible by using the immunostimulatory CpG. Fan *et col.* developed NCPs made of tryptophan-phenylalanine dipeptide with Zn(II) ions [53]. The synthesised NCPs showed fluorescence in the visible range and excellent stability and biocompatibility. Worth to mention, these NPs were able to incorporate Dox through π-π stacking that could be released *in vitro* (50% in 24 h, pH 6.0) as monitored by fluorescence. Finally, Bertleff-Zieschang *et col.* reported the self-assembly of different flavonoids and Fe(III) ions as films or microcapsules with high antioxidant activity retained for several cycles [54].

No disregard for the examples above, Pt(IV)-based CPs are without doubt one of the most visible cases of chemical entrapment as pioneered by Lin *et col.* (*vide infra*) [55]. Other authors such as Yuanfeng *et col.* described PEG-coated NCPs made of Zn(II) and alendronate (ALN) to deliver the prodrug c,c,t-(diamminedichloro disuccinato)Pt(IV) (DSP) [56]. *In vivo* biodistribution studies demonstrated a preferential platinum delivery in metastatic than in healthy bones (4-fold), reducing side toxicity effects. The benefits of these NPs was confirmed by Adarsh *et col.* who showed a different and more effective action mechanism than cisplatin and the free Pt(IV) prodrug [43].

Another family of effective chemical entrapment is that represented by antitumour nitrogen-containing bisphosphonates (N-BPs), which inhibit matrix metalloproteinase activity and down-regulate integrins [57]. The main limitation of N-BP was its quick renal clearance and strong bone binding. To avoid this, different N-BPs, including pamidronate or zoledronate, were also used in combination with Ca(II) ions, which were further coated with cationic lipid bilayers to increase their stability [58]. The formed NCPs were gradually destroyed under physiological conditions with a sustained release, from a few to 120–140 h. The *in vitro* cytotoxicity assays on H460 cell lines revealed very low IC_{50} values (4.5–1.0 mM) upon integrating the lipid bilayers with the cell membrane [59].

To end this section, we would like to point out a novel approximation recently reported consisting in the chemical modification of drug-based ligands that are cleaved under physiological conditions. So far, it has been mainly used to synthesise efficient NCPs platforms to treat AIDS/HIV [60]. The strategy consisted of functionalizing azidothymidine (AZT, an anti-HIV drug) with a chelating catechol group, incorporating a spacer cleavable under enzymatic hydrolysis. Worth to mention that this approach could be extended to antitumoural applications, ensuring bigger encapsulation yields and better control of the release kinetics.

3. Stimuli-responsive NCPs

Another critical issue is developing responsive NPs that selectively deliver the drug in a controlled ON-OFF manner. Next, the different approaches described in the literature are revised.

3.1. pH-responsive

pH stimuli is relevant mainly due to two reasons. First, coordination bonds can be sensitive to pH variations, especially at low pH, where protonation of the ligand takes place. Second, such sensitivity can be used to target the release, while reducing side effects, taking advantage of the variations within intra- and extracellular environments in cancer cells. The different examples are categorised next by families of metal ions and/or ligands.

3.1.1. Metal node

Iron. Gao *et col.* reported NCPs encapsulating Dox hydrochloride (40% drug loading content) made of Fe ions coordinated to 1,1′-(1,4-butanediyl)bis(imidazole) and subsequently coated with silica [46]. The NPs revealed the sustained release of the drug for more than a few days, notably faster at low pHs. Fe(III)-gallic acid (GA) NCPs encapsulating up to 93.5% of Dox, which was released at the lower pH of the lysosomes, were also stated [61]. Not only that, but the NPs also exhibited an efficient *in vivo* tumour growth inhibition. In another example, Xu *et col.* proposed core–shell Fe_3O@ salphen-In(III) CP [62]. At pH 5.0, the Fe_3O_4 core slowly released Fe ions. These ions coordinated with the released salphen ligands as active drugs, exhibiting IC_{50} values competitive with pharmaceutical Mn(II)-salen drugs.

Copper. Bai *et col.* described the polymerisation of histidine, Dox and Cu(II) with high drug loadings and pH-dependence release (pH 5.0) due to the dissociation of the coordination bonds [63]. Finally, Wang *et col.* reported the production of NCPs based on Cu(II) and dioxocyclam, which were dissociated at low pH [64].

Other metal ions. Wang *et col.* described the formation of titania nanotubes (TNTs) loaded with active ibuprofen, vancomycin, or Ag NPs [65]. The systems were fabricated using bix and Zn(II) (osteoblastic proliferation) or Ag(I) ions (antibacterial), allowing for the release of the cargo at low pH due to degradation of the NCP. Alternatively, Zn-based hexahistidine NPs with low cytotoxicity, fast internalisation and high loading capacities (up to 53%) were described by Huang *et col.* [66]. Specifically, the antitumoural camptothecin (CPT) encapsulation resulted in more effective performance than the free drug. Interestingly, the formed NCPs showed a sustained release at pH 4.5. Yang *et col.* also published NPs made of a cisplatin Pt(IV) prodrug bearing two carboxylic groups, poly-L-histidine-PEG and Ca(II), Co(II), Ni(II), Hf(IV) and Tb(III) ions [67]. While stable at neutral pH, a fast release was observed at low pH, favouring *in vitro* and *in vivo* therapeutic effects at low doses (Fig. 5).

3.1.2. Ligands

Phenol family. Using different templates, Ejima *et col.* reported non-toxic tannic acid (TA) and Fe(III) capsules that decomposed in acidic pHs [68]. Interestingly, the reported NCPs exhibited permeability, stiffness, good degradability [69] and Dox encapsulation [70]. For instance, pH-dependent capsules made by reaction of TA with Al(III), Mn(II), or Gd(III) showed an effective cell internalisation carrying several anticancer drugs (irinotecan, topotecan, or verapamil). Beyond TA, catechols have also been successfully used. Li *et col.* reported the combination of Fe(III) ions, hydrocaffeic acid, Dox and dopamine-modified hyaluronic acid [71]. The phenolic-based NCPs showed tumour growth inhibition without recurrence, thanks to the Dox release at the low pH in endosomes/lysosomes or near-infrared (NIR) induced phototherapy [72]. Combinations of polyethyleneglycol (PEG), catechol-functionalized hyaluronic acid and Dox showed pH-induced drug release and targeting for CD44+ cancer cells. These results were improved, supported by additional protein corona effects [73]. Park *et col.* used this same approach to coat yeast cells without losing their biological activity [74].

In an interesting work, oleic acid emulsions containing Dox were coated with a PEG holding catechol groups and Fe(III) ions that respond to pH [75]. The obtained NPs exhibited high cytotoxicity in human breast cancer cells, good permanence in the bloodstream and a stealth-like response.

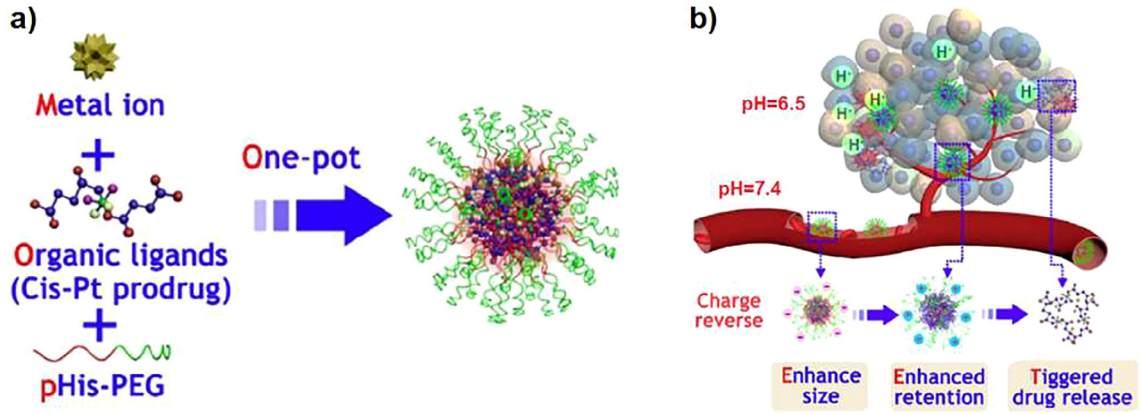

Fig. 5. a) one-pot synthesis of PEGylated NCPs and b) application as pH-responsive anticancer therapy favoured by the enhanced permeation and retention (EPR) effect. Reproduced from Ref. [67] with permission of the copyright holder.

pH-sensitive ligands. An acid-sensitive imine linker together with Hf(IV) was used by Liu *et col.* to obtain NCPs capable of encapsulating chloro(triphenylphosphine)gold(I) (TPPGC) [76]. The NPs exhibited excellent stability in physiological conditions and were degraded in acidic environments, releasing the drug *in vitro* and *in vivo*. Moreover, the chemotherapy was fully implemented with the radiosensitisation of the Hf ions without compromising the toxicity nor the biodegradability. The same imine-based linker was reacted with Mn(II) ions and PEG by Liu *et col.* to obtain NPs encapsulating collagenase that degraded at low pH, exhibited high tumour accumulation and photodynamic effects [77]. Finally, Nador *et col.* have synthesised NPs made of Co(II) ions and a bis-catechol ligand bearing pH-dependent imine group [78]. The NPs were stable at neutral pH but degraded and aggregated at pH 5.0.

3.2. Photoactivation or redox stimuli

Zhang *et col.* fabricated NCPs by the combination of Zn(II) and a bis(imidazole) ligand encapsulating fluorescein, tetracycline (antibiotic), or Dox [79]. The encapsulated cargos were selectively released upon UV light irradiation thanks to the presence of a photocleavable *o*-nitrobenzyl unit. Accordingly, cytotoxic effects in HeLa cells were further substantial upon irradiation. In another example, Liu *et col.* described the reaction of the singlet-oxygen sensitive bis-(alkylthio) alkene linker (BATA) with Hf(IV) ions to generate NCPs loaded with the photosensitiser chlorin e6 (Ce6) and Dox [80]. Therefore, red light induced both the formation of singlet oxygen and the drug release after ligand rupture and NP degradation. Moreover, *in vivo* distribution showed good tumour accumulation and synergistic chemo/phototherapy more efficiently than independently administered drugs. Finally, Hu *et col.* described NCPs using Zn(II) and a photoswitchable diarylethene ligand (UV or visible), representing a new paradigm for light-triggered release [81].

On the other side, GA and Fe(III) based NCPs with redox-controlled degradation, and therefore tunable drug release, was reported by Cherepanov *et col.* [82]. Micelles made of PEG-poly(N (2-hydroxypropyl)methacrylamide bearing 4-(methylthio)benzoyl groups and the [ethylenediamineplatinum(II)]$^{2+}$ linker were shown to effectively encapsulate curcumin [83]. Interestingly, after treatment with dithioerythritol, the drug release was favoured, mimicking the intracellular glutathione (GSH).

3.3. Stimuli combination

The combination of two or more stimuli allows for better control of the cargo release. In this sense, Li *et col.* described the formation of chemically and colloidally stable Zn(II) and histidine-containing dipeptide NCPs [84]. The NPs showed the release of Ce6 (encapsulation yield higher than 50%) in front of both pH- and GSH. The NPs also exhibited excellent *in vivo* circulation lifetimes and antitumour accumulation and efficacy with very low toxicity. In the example shown in Fig. 6**,** Liu *et col.* described the formation of MnO_2 NPs coated with the Hf(IV) and the Pt(IV) prodrug DSP CP and PEG [85]. The presence of the Hf(IV) ions ensured the radiotherapy, the MnO_2 NPs, the magnetic resonance imaging (MRI), and the Pt(IV) prodrug the chemotherapy once released in the reductive intracellular environments. The system was evaluated *in vivo*, showing features as chemotherapeutic with no appreciable side toxicity.

Continuing with the examples, core–shell NPs combining PEG-poly(4-vinylpyridine), folic acid and the Ir(III)-2-phenylquinoline complex were shown to interact with histidine intracellularly, releasing the iridium complex that acts as an active drug and a phosphorescent emitter [86]. The reaction of Eu(III) or Tb(III) ions with guanosine 5′-monophosphate (GMP) resulted in NPs with controlled release of *N*-methyl mesoporphyrin IX (NMM), as followed by fluorescence [87,88]. GMP was also reacted with lanthanides by Gao *et col.* to report NCPs that responded to dipicolinic acid, ethylene diamine tetraacetic acid, pH and Cu(II) or Hg(II) ions [89]. To finish with this section, Bai *et col.* synthesised NCPs with a disulfide-Dox prodrug and Cu(II) that responded to the simultaneous presence of the reductive/acidic environments of tumoural cells [90].

4. Metal chemotherapy

4.1. Platinum-based drugs

Undoubtedly, one of the utmost active metal ions used for the assembly of NCPs is platinum. In fact, cisplatin and other Pt(II) anticancer drugs, such as carboplatin or oxaliplatin (OxPt), are already FDA-approved chemotherapeutics used for a long-time treatment of several different cancers [91]. Due to this success, scientists also aimed to include in clinical experiments other Pt(II), Pt (IV) prodrugs and photoactivatable Pt(IV) [92], with a wealth of optimism based on NPs for future platinum-based cancer drugs [93]. From all of them, Pt(IV) prodrugs are the ones mostly used

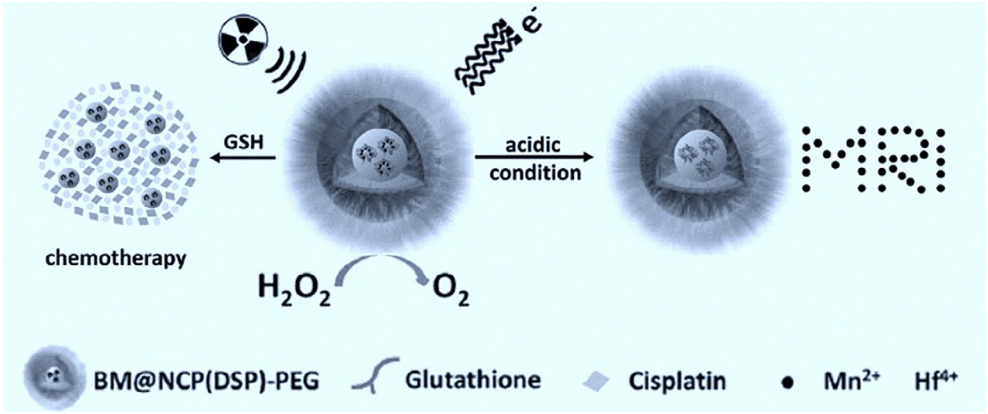

Fig. 6. Schematic representation of the theranostic and redox/pH responsive MnO_2 NPs coated with a CP shell formed by Hf(IV) + c,c,t-(diamminedichlorodisuccinato)Pt(IV) (DSP). Drug release responds to a pH decrease, reductive environments, and endogenous tumour H_2O_2, enhancing cancer chemoradiotherapy. Moreover, these NPs are able to tumour-specific magnetic resonance imaging (MRI). Reproduced from Ref. [85] with permission of the copyright holder.

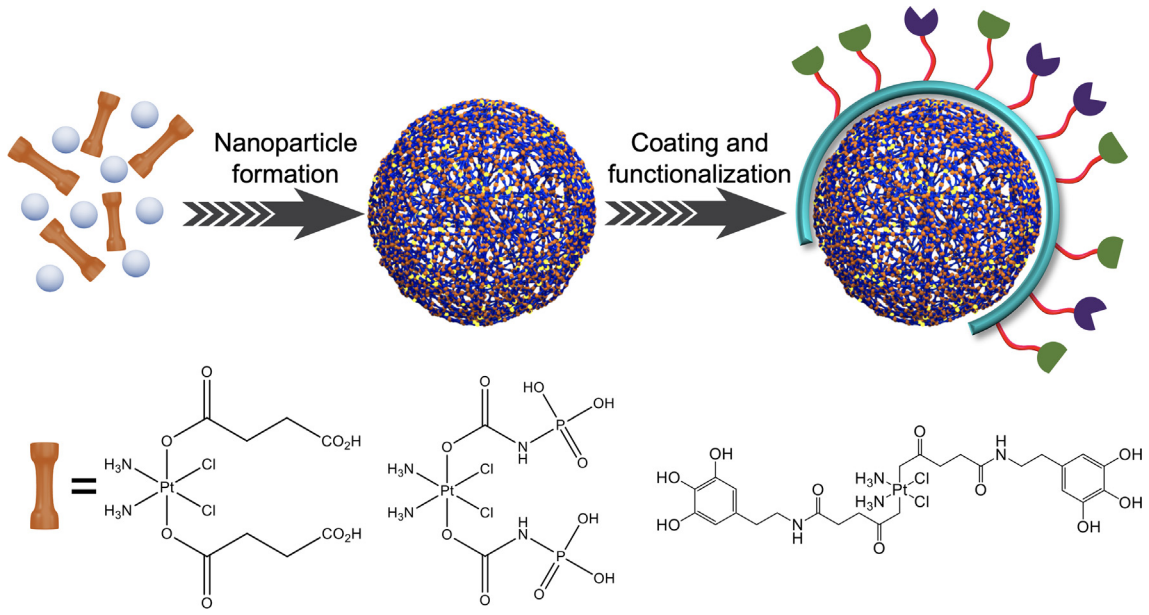

Fig. 7. Schematic representation of the NCPs formation using the Pt(IV) prodrugs (top) shown in three leading families of Pt(IV) prodrugs used as synthons in the building of NCPs (bottom).

to obtain NCPs combined with bis-chelating equatorial ligands able to further coordinate with other metal ligands [94]. Beyond inducing the polymerisation, axial ligands can also introduce additional properties and/or biological activity. Mainly three different families of ligands, schematically represented in Fig. 7, have been used with this aim.

4.1.1. Succinate (DSCP)

A seminal work published in 2008 by Lin *et col.* described cytotoxic effects in colon and breast cancer cells of NCPs synthesised from terbium metal ions and the DSCP ligand [55]. Further coating with a silica layer functionalised with a silyl-derived peptide RGD provided both cell targeting properties and controlled release of the cisplatin prodrug. Later on, the silica coating was replaced by a lipid bilayer, bearing the active targeting molecule anisamide (AA), which improved the biocompatibility and cytotoxicity in human cell lung cancer cells [95]. The same group has also reported NCPs loaded with GMP and carboplatin (8.6 ± 1.5 wt% and 28.0 ± 2.6 wt%, respectively) with a robust synergistic effect to treat Pt-resistant OCa cells [96]. *In vivo* studies also showed persistent circulation in the bloodstream and improved tumour uptake, resulting in tumour growth inhibition (80%) and regression (70%).

In another example, Zhao *et col.* used NCPs made of Zn(II) coordinated to alendronate (ALN) and a fatty acid-modified PEG to efficiently deliver DSCP to the bone [56]. For this, particle size was regulated by adjusting experimental parameters down to approximately 55 nm to extravasate into capillaries and accumulate into metastatic bones. Besides, to efficiently inhibit tumour growth, these NPs also reduced osteoclastic bone destruction with no significant toxicity. More recently, a new biodegradable NCP family incorporating Fe(III) and DSCP, which was liberated in the presence of GSH, was reported [97]. Interestingly, the Fe(III) ions were reduced into Fe(II), which enforced an amplified intracellular oxidative stress via the Fenton reaction. Further decoration of the NPs with PEG and the cyclo[Arg-Gly-Asp-D-Phe-Lys(mpa)] peptide

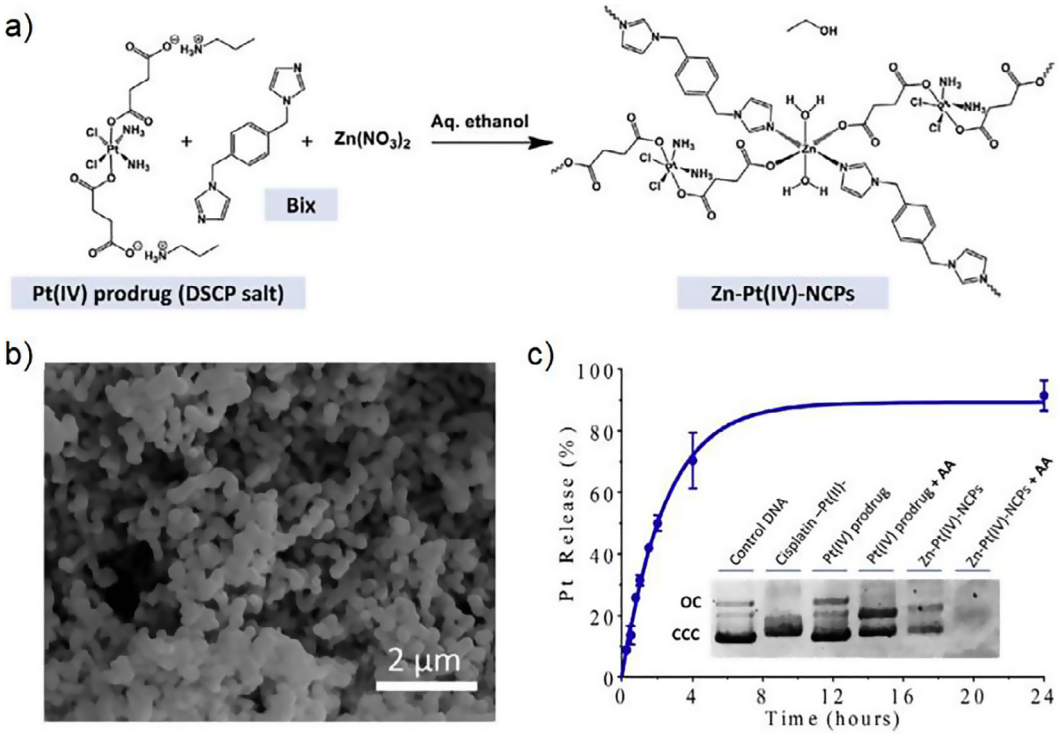

Fig. 8. a) synthesis of Zn-Pt(IV) and b) SEM image of Zn-Pt(IV) NCPs; c) *in vitro* platinum release kinetics and agarose gel electrophoresis of a *pBluescript II* plasmid DNA treated with the NCPs, the free prodrug and blanks (inset). Reproduced from Ref. [43] with permission of the copyright holder.

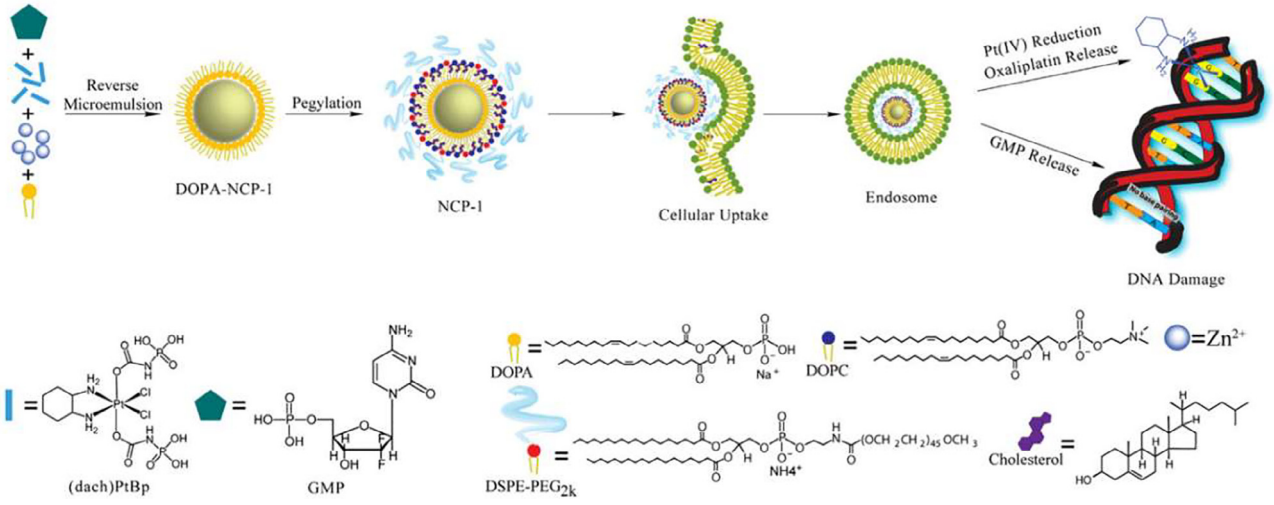

Fig. 9. Graphic illustration of the fabrication, composition and effect of Pt-based NCPs, showing the endocytosis and release of OxPt and GMP, and the OxPt and GMP based DNA replication disruption. Reproduced from Ref. [99] with permission of the copyright holder.

(cRGD) enabled an excellent targeting effect against $\alpha v\beta 3$-integrin, which is commonly overexpressed in tumoural cells, showing outstanding biosafety and biodegradability.

Even though successful, previous examples lacked mechanistic details that justify its effectiveness, the reason why some of us decided to gain more in-depth knowledge on how nanostructuration modulates the mechanism of actuation of platinum-based drugs. For this, we designed NCPs made of a Pt(IV) prodrug, Zn (II) and bix ligand (Fig. 8) [43].

The formed NPs (with a size around 200 nm) exhibited excellent permanency in physiological media and sustainable control drug release. Moreover, Pt(IV)-based NCPs demonstrated enhanced cytotoxicity with respect to free Pt(IV) prodrug in neuroblastoma cells, cervical cancer, and human adenocarcinoma. Such improvement does not come from a differential Pt cell uptake but a higher DNA bonding. The results showed how the nanostructuration could adjust the bioavailability of different species to enhance the therapeutic action compared to the free drug.

4.1.2. Phosphonic acid

NCPs made of biphosphonic acids containing cisplatin and OxPt with high drug loadings (~48 and ~45 wt%, respectively) and a coating combining lipids and PEG were reported by Lin *et col.* [98]. These NCPs revealed low activation of the mononuclear phagocyte system and, therefore, a considerable blood circulation time that allowed for their use to treat subcutaneous tumour mur-

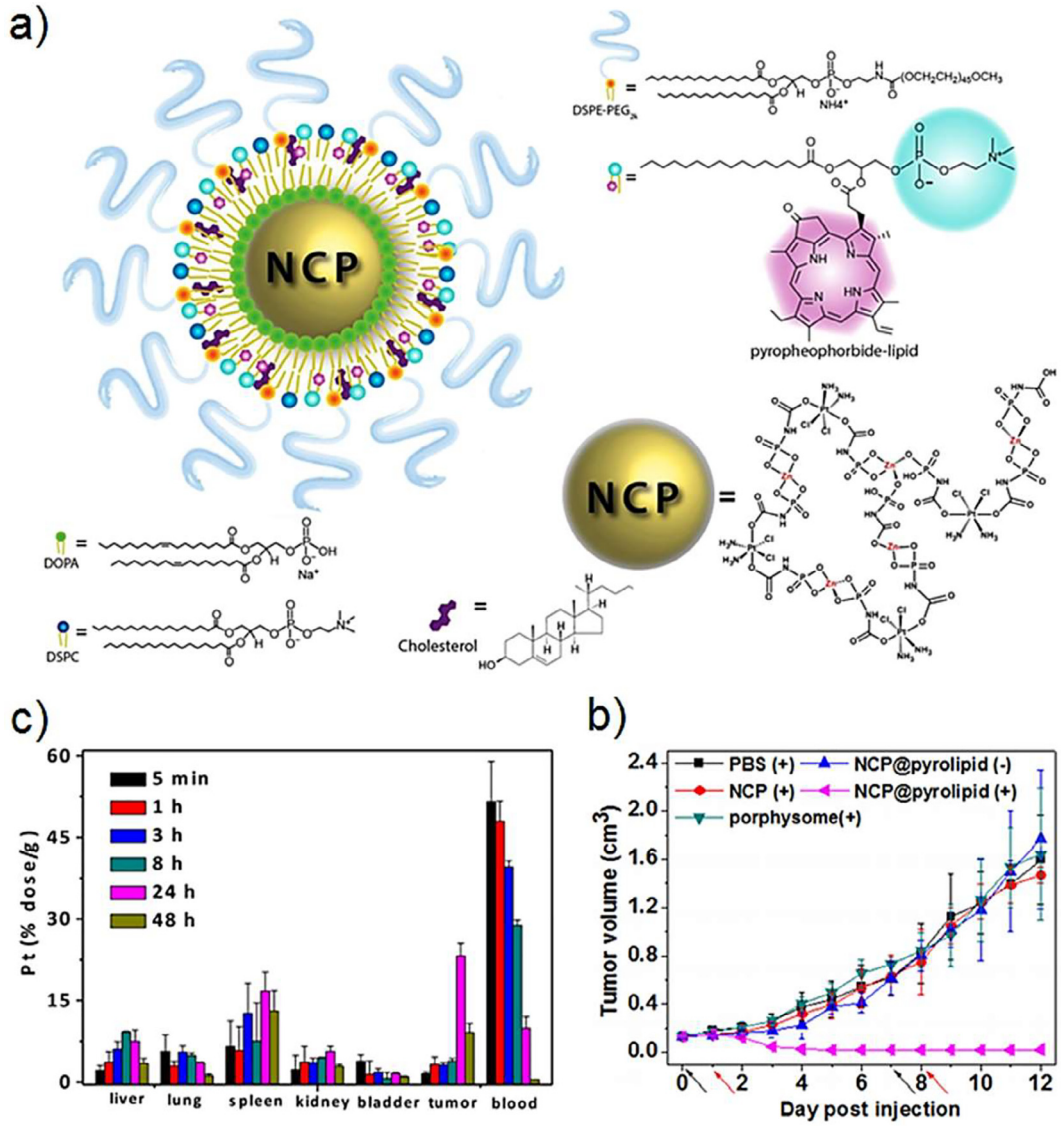

Fig. 10. a) representation of NCP@pyrolipid NPs, including PEG in the coating layer; b) intravenous (i.v.) injection and tissue distributions of Pt released from NCP@pyrolipid; c) tumour development inhibition curve after i.v. injection of phosphate-buffered saline (PBS), NCP, porphysome, or NCP@pyrolipid to the human head and neck cancer SQ20B subcutaneous xenograft murine models. Reproduced from Ref. [100] with permission of the copyright holder.

ine models with higher efficacy than free drugs. This approach was likewise useful to combine different chemotherapeutic approaches within a single nanocarrier. For instance, Zn(II)-based NCPs with OxPt and gemcitabine monophosphate (GcMP) ensured a synergistic effect in pancreatic cancer mouse models (Fig. 9) [99]. In addition to minimal mononuclear phagocyte system uptake and prolonged bloodstream circulation, these NPs ensured the co-delivery of both anticancer drugs with different action mechanisms to concurrently disrupt several anticancer mechanisms.

Yet again, Lin *et col.* described core–shell NCPs containing high loads of cisplatin and a pyrolipid (photosensitiser) for combined chemo-/photodynamic therapy (PDT) [100]. These NPs showed superior and efficient tumour reversion in head and neck cancer-induced mouse models (83% tumour reduction) compared to administering the non-encapsulated anticancer drugs (Fig. 10).

Another emergent area where NCPs point to success is in immunotherapy for cancer treatment [101]. With this aim, previous NCP-pyrolipid nanoformulations were combined with the *PD-L1* antibody to treat subcutaneous CT26 and HT29 mouse models by generating a strong tumour-specific immune response combined with the PDT effect [102]. Significant immunotherapy effects were also obtained using lipid-coated NCPs that systematically delivered a combination of OxPt and dihydroartemesinin (DHA). This system effectively induced cell death through the synergism of ROS and the anti-*PD-L1* antibody in murine colorectal cancer tumours [103].

Different examples of RNA-bearing NPs have also been described. For instance, self-assembled NCPs with the cisplatin prodrug coated with a cationic lipid layer occluding siRNAs have been reported to target three multidrug resistants (MDR) genes that overcome cisplatin-resistance ovarian cancer cells [104,105]. Cell viability studies showed an improved chemotherapeutic efficacy by downregulating the expression of MDR genes while the *in vivo* local administration reduced tumour dimensions of subcutaneous xenografts. Finally, non-toxic NCPs based on Pt(IV)$(en)_2$-bis(phosphonic acid) [en = ethylenediamine] and microRNA (miRNA) were coated with a self-assembled lipid bilayer [106]. Subsequently, the resulting system was functionalised with PEG chains, avoiding the clearance by phagocytes.

4.1.3. Gallate

Beyond succinic and phosphonic acid, the tendency over the last few years has been the introduction of gallate groups, favouring the coordination with metals and providing additional anticancer properties. In this direction, in 2017, Caruso *et col.* reported PEG-modified NPs (≈100 nm) with antifouling and high drug loadings [107]. The NPs exhibited long *in vivo* circulation times (half-life of ≈18 h) and better (up to four times) antitumour activity in a human prostate cancer xenograft mouse model compared with the prodrug or cisplatin. One year later, Chen *et col.* reported the protection of phagocytic enzyme myeloperoxidase (MPO) from degradation by coating with pPt/PEG polyphenols [108]. The NPs, which exhibited excellent *in vivo* blood circulation and tumour retention, improved the efficacy as the Pt ion produced H_2O_2 that MPO intercellularly catalysed into the active HOCl. In another successful example, a combination of chemo-photothermal therapy (PTT) with multimodal photoacoustic (PA)/MRI/positron emission tomography (PET) imaging was achieved by using NPs made of the Pt prodrug polyphenol and Gd(III) ions. In these NPs, coated with the pH/sensitive PEG-based block copolymers, the Pt drug release was activated under NIR irradiation or in the characteristic acidic pH of tumours. The results showed enhanced MR signal, exhibiting an excellent tumour accumulation and eradication with low power NIR laser irradiation [109]. Finally, the combination of epigallocatechin-3-gallate (EGCG, a Pt(IV) prodrug bearing phenol groups) and polyphenol modified PEG block copolymers, using Fe(III) as a metal node, yielded NPs with a relevant cellular internalisation. Cisplatin was also used to increase the intracellular H_2O_2 necessary to generate reactive oxygen species (ROS) through the Fenton reaction of the Fe(III) ions and, therefore, a chemodynamic/chemotherapy anticancer efficacy [110].

The examples previously reported, though successful, still exhibited intrinsic resistance to some tumours and mainly adverse side effects. For this reason, more efficient metal-based therapeutic agents, some of them being currently running clinical trials, are actively being searched nowadays [111]. Growing developments based on Ru, Cu, Zn, Au, or In complexes have received intensive attention over the last years [112–114].

4.2. Copper-based drugs

In the case of copper, there are enough examples to configure a specific section. One of the first reports appeared back in 2011; Arunachalam *et col.* reported NCPs made of copper ion and bipyridyl/polyethyleneimine ligands that killed NCI-H460 human lung cancer cells [115]. One year later, Wang *et col.* reported Cu-aminobenzoate NPs with IC_{50} values of 17.5 ± 4.9 and 30.7 ± 1.3 μg/mL at 72 h for HeLa and NCI-H446 cells, respectively [116]. These toxicities were related to the released Cu(II) ions from NCPs and/or direct interaction of the NPs with the cells. Other Cu-based NCPs containing 1,10-phenanthroline and L-arginine induced the apoptosis of MCF-7 mammary carcinoma cells, most likely due to the formation of DNA/RNA complexes [117].

More recent efforts aim for the integration of different strategies and drug combinations pursuing synergistic antitumoural effects. In this sense, Wu *et col.* designed multifunctional NCPs that consisted on hyaluronic acid (targeting), AQ4N (chemotherapeutic), gossypol (chemotherapeutic agent and a self-carrier) and Cu (II) as connecting node and antitumour enhancer [118]. These NPs (88.7 ± 7.4 nm) exhibited excellent drug encapsulation efficiencies (70–100%) and tumour-targeting abilities mediated by hyaluronic acid receptors and pH. *In vivo* experiments showed that the NPs accumulated and released drugs specifically at the tumour region, favouring a considerable decrease of the administered dose and any related side effect. Liu *et col.* reported AQ4N-Cu(II) NPs combining now banoxantrone and Dox [119]. The anticancer drug was delivered through a pH-sensitive release in the tumour microenvironment facilitated via microvesicle-mediated intercellular transfer. Moreover, the release was traced by the fluorescence of the released AQ4N or Dox upon protonation. Thus, these NCPs were capable of loading phthalocyanine and induced the PDT "on-demand", which facilitated a hypoxic atmosphere and triggered the decrease of AQ4N, increasing therapeutic efficiency.

4.3. Other metal-based drugs

Many Ru(II)-based inorganic and organometallic complexes have relevant therapeutic action [120], though only a few are NCPs. Higuchi *et col.* reported supramolecular NCPs combining bis(terpyridine) with Ru(II)/Fe(II) that significantly inhibited the growth of cell lung cancer lines (NCI-H460) thanks to metal/phosphate ion interactions with the DNA [121]. Raja *et al.* used $Co(NO_3)_2$ and isonicotinic hydrazine that interacted with calf thymus DNA and bovine serum albumin (BSA) [122]. This system exhibited strong radical scavenging potency and cytotoxicity against Hep-2, Hep G2, HeLa and A431 cancer cell lines (two/three times higher when compared to cisplatin). Correlation of the binding ability of cobalt complexes, DNA and inhibition values were, later on, confirmed [123], as well as Cu(II) and Zn(II) [124]. Different substituents and other structural changes influenced the activity, bringing invaluable information to the strategy of efficient agents for targeting nucleic acids. In another family of examples, arsenic and bismuth-based polymers were shown to be very effective (low IC_{50} values), inhibiting the growth of the human prostate cells while exhibiting low toxicity towards normal human cells (Fig. 11) [125,126].

Researchers also studied the anticancer activity of La(III), Sr(II) [127] and In (III)-based [128] NCPs. On top of that, some precious metal-containing polymers also showed engaging anticancer activities following mechanisms different from those of Pt-based polymers [129]. However, their use has been scarcely explored as rigid chelation is required to achieve stability [130]. Finally, the nanostructuration of kinetically inert coordination complexes for anticancer agents, such as Rh(III) or Ir(III) [131], could open interesting investigations for anticancer activity. To conclude this section, Huang *et col.* rationally designed NCPs incorporating GSH-responsive NO donor and Fe ions [132]. Degradation of the NO donor in the presence of GSH in tumour cells (~10 mM) quickly reacted with H_2O_2 and O_2^- anions to form peroxynitrite anion ($ONOO^-$) and, therefore, enhanced the chemodynamic efficacy (Fig. 12).

5. Photodynamic therapy

PDT lies in the administration of photosensitiser in a tumour area, which under light activation generates singlet oxygen ($^1O_2$) that activates cell apoptosis/necrosis and immunity [133]. One of the main advantages of using NPs for this therapy is that the photosensitiser is accumulated in the tumour cells. Therefore, irradiation can selectively generate a local amount of ROS, preserving surrounding tissues. In the case of CPs, most of the examples so far reported are NMOFs [134–137], with some interesting NCPs reported. For instance, nanostructuration has been found to solve the low solubility and selectivity of Zn phthalocyanine-based photosensitisers [138]. Zhao *et col.* designed NCPs from the coordination between phthalocyanines and Zn(II) [139]. The resulting systems were coated via self-assembly of a lipid bilayer that generated PDT in MCF-7 cell cultures and cholesterol derivatives that ensured responses to acidic tumour microenvironments. In another example, Chen *et col.* reported NCPs embracing DNA coordinated to Ca(II) with AS1411 DNA G quadruplexes and

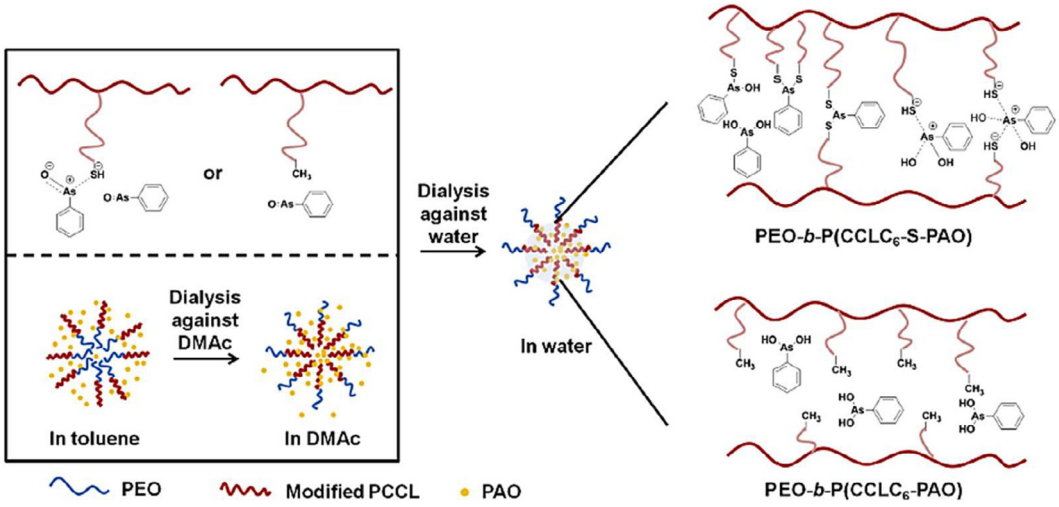

Fig. 11. Encapsulation of phenylarsine oxide (PAO) into a biodegradable block copolymer containing pendant thiol groups (or not) on the hydrophobic part; i.e., [PEO-b-P(CCLC6-SH)]PEO-b-P(CCLC6-SH) and PEO-b-P(CCLC6) micelles. The upload process takes place upon solvent polarity changes, while arsenic was entrapped chemically (reaction with the thiol groups) or physically in the polymer that did not contain the thiol groups. The detachment of PAO from PEO-b-P(CCLC6-S-PAO) took place by direct hydrolysis in aqueous media or by glutathione (GSH) triggered arsenic release. Reproduced from Ref. [126] with permission of the copyright holder.

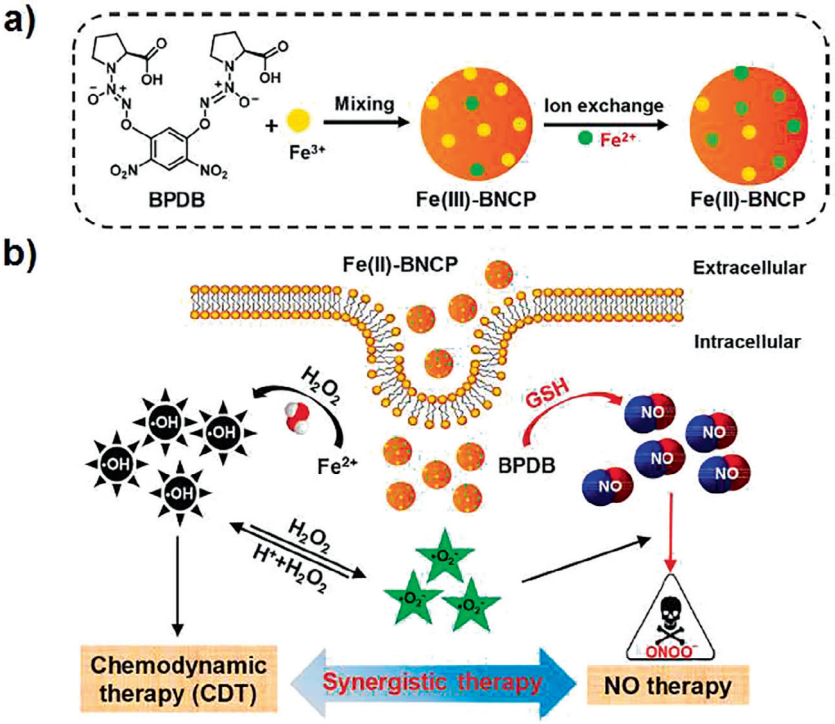

Fig. 12. a) synthesis of Fe(III)-BNCP NPs; b) tentative mechanism for the NO chemodynamic activity of these NPs in tumour cells. Reproduced from Ref. [132] with permission of the copyright holder.

pHis-PEG, and the additional incorporation of the photosensitiser Ce6 and an Fe-containing porphyrin (hemin) [140]. With further PEG modification, the nanostructure demonstrated cell internalisation and intranuclear ROS activity. Simultaneously, the PDT effect was improved through the inhibition of anti-apoptotic protein B-cell lymphoma 2 expression. Interestingly, endogenous tumour H_2O_2 could decompose the DNAzyme function (Fig. 13).

In a similar approach, Chu *et al.* assembled porphyrin/G-quadruplex complexes (with NIR light responses) on NCPs resulting from the coordination of Zn(II) ions with an amphiphilic amino acid [141]. The final NCPs were coated with an anti-nucleolin aptamer (AS1411), which improved cancer cell-targeted capability in different cancer cells. *In vivo* assays showed a significant accumulation into tumours through the EPR effect, aptamer interaction with tumour markers and NIR-induced PDT. The nanoassembly could also disassemble inside the acidic tumours containing GSH, so the porphyrin/G-quadruplex tandem was more effective while reducing the $^1O_2$ consumption of the GSH.

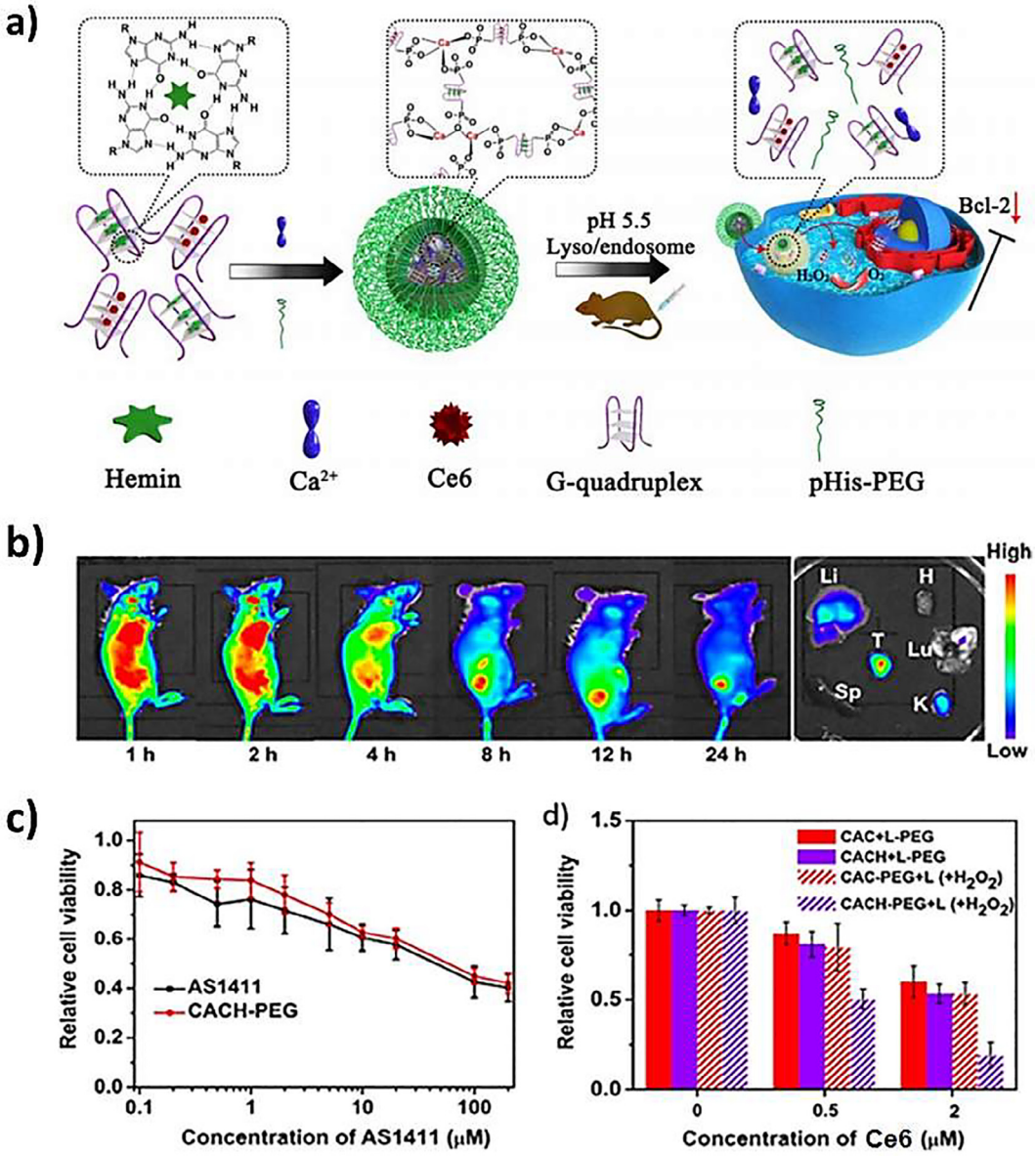

Fig. 13. a) scheme of Ca-AS1411/Ce6/hemin@pHis-PEG (CACH-PEG) NCPs; b) time-dependent *in vivo* fluorescence imaging of 4T1 tumour-bearing-mice after i.v. injection (right column: *ex vivo* imaging of different organs and tumour took after 24 h post-injection from a representative mouse); c) Viability of 4T1 cells treated (72 h) with different concentrations of AS1411 or CACH-PEG; d) viability of 4T1 cells incubated with CAC-PEG or CACH-PEG and irradiated with 660 nm light (5 mW/cm^2, 30 min) with and without 100 μM H_2O_2. *L* stands for a sample exposed to a 660 nm LED irradiation at a density of 5 mW/cm^2. Reproduced from Ref. [140] with permission of the copyright holder.

6. Unconventional approaches

One of the significant difficulties in treating cancer comes from the extracellular matrix that prevents the tumour diffusion of drugs and favours hypoxic environments unsatisfactory for efficient treatments. Therefore, developing strategies to degrade the extracellular matrix is expected to improve existing cancer therapies. With this aim, Liu *et al.* encapsulated collagenase in PEG-coated NCPs made of Mn ions and a benzoic-imine ligand sensitive to pH. These NPs efficiently accumulate in the tumour and release collagenase thanks to the acidic pH that degraded collagen and minimise the extracellular matrix [77]. Wang *et al.* recently published an interesting idea to combat metastatic cancer by regulating the immune system using vaccine-like microparticles made of epigallocatechin-3-gallate (EGCG) and Al(III) metal ions and encapsulating tumour cells (Fig. 14) [142].

Changing the approach, Mirkin *et col.* reported the synthesis of NCPs, based on the reaction of $Fe(NO_3)_3$ and 3-hydroxy-4-pyridinone (HOPO) conjugated with DNA as biocompatible gene-regulation agents [143]. The resulting nanoconjugates showed the ability to enter cells and target a known cancer-related mRNA transcript (SKOV-3 ovarian-cancer cells) that modified protein expression without the need for transfection agents, generating an efficient gene knockdown. Alternatively, Liu *et col.* described biodegradable NCPs for radioisotope therapy in clinical cancer treatments [144]. The proposed nanosystem consisted on PEG-modified NCPs obtained by the one-pot reaction of Hf(IV) ions and tetrakis (4-carboxyphenyl) porphyrin (TCPP). These NPs could be simply labelled with ^{99m}Tc(IV) (radioisotope with a half-life of 6.0 h) that emit γ rays, resulting in NPs feasible for SPECT imaging. The results revealed efficient *in vivo* tumour retention and elimination with moderate doses of ^{99m}Tc. On top of that, the NPs were

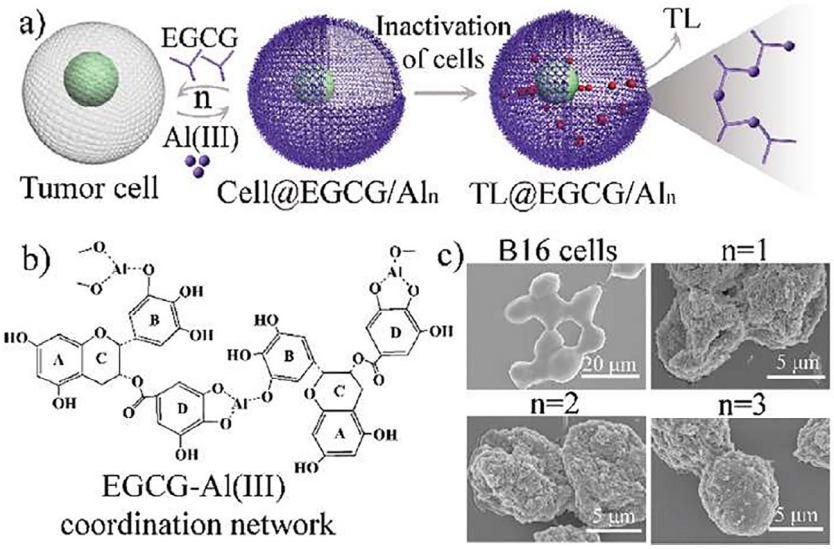

Fig. 14. a) schematic representation of tumour cells coated with an EGCG/Al layer (TL@EGCG/Al_n); b) expected coordination modes within the NP; c) SEM micrographs of uncoated B16 cells and different coating tumour cells. Reproduced from Ref. [142] with permission of the copyright holder.

biodegradable and easily excreted without significant long-term body accumulation, indicating their promising effect for cancer radioisotope therapy. Interestingly, the NCPs allowed for improved efficacy and fewer side effects than currently used radioisotopes (half-lives of days).

Hybrid NPs combining gold nanosystems and a CP obtained by reaction of $(pq)_2Ir(Hdcbpy)$ with $Dy(OOCCH_3)_3$ have been reported [145]. The hybridisation of both induced an evident redshift of the local surface plasmon resonance peak. Furthermore, these hybrid NPs also exhibited PAI-induced NIR-driven PTT and MRI *in vivo*. Finally, in another work, Li *et col.* described the formation of hybrid NPs by combining DNA and Fe(II) ions that released DNA *in vitro* and *in vivo* [52].

7. NCPs for theranostics

There are a plethora of examples describing the use of NCPs as imaging systems [146]. One of the cornerstones in cancer research nowadays is the combination of drug efficacy with tumour monitoring in real-time to increase the safety of the treatment [147].

7.1. MRI and chemotherapy

MRI is an effective non-invasive procedure that allows for excellent imaging resolution and body penetration. Commonly, MRI requires the administration of external CAs to enhance image resolution and efficacy. Next, we revise examples of NCPs grouped according to the metal ion used.

7.1.1. Gadolinium-based NCPs

Zhu *et col.* developed biodegradable gadolinium NCPs loaded with Dox stable at neutral pH but responsive to pH modifications [148]. The presence of the CD44 receptor in the NPs facilitated the selective internalisation and trapping within acidic partitions of HeLa cells. Once there, the NPs disassembled, releasing Gd ions and fluorescent Dox used for real-time monitoring. Ma *et al.* engineered NPs for theranostics merging amphiphilic pluronic F127 and a peptide-amphiphile with drugs located into the hydrophobic micelle cores and chelated with Gd(III) MRI CAs [149]. Experiments on tumour-bearing mice using Dox demonstrated them as efficient therapeutic agents. Recently, examples of Dual-Mode Contrast Agents (DMCAs) NCPs to facilitate the understanding of diagnostic images by suppressing MRI artefacts and ambiguities, have been effectively obtained. Yang *et col.* developed multifunctional Gd (III)-based NCPs combining 1,1′-dicarboxyl ferrocene, coated with silica to improve water stabilisation and superficial amination [150]. Surface amine groups allowed for the covalent coupling of a fluorescent rhodamine dye (RBITC) and an arginine-glycine-aspartic acid (RGD) peptide resulting in water-stable NCPs with low cytotoxicity and dual-mode T_{1w}/T_{2w} *in vivo* imaging (Fig. 15).

7.1.2. Manganese-based NCPs

Lin *et col.* reported Mn-bisphosphonate NCPs with remarkable loads of zoledronate (63 wt%) and Mn(II) ions (13 wt%) [151]. The NPs were further coated with lipids, PEGylated and functionalized with anisamide to enable specificity to cancer cells, biocompatibility and control over the drug release. *In vitro* MRI assays evidenced the efficacy of these NCPs as an efficient CA and validated the targeting ability and apoptosis in breast/pancreatic cancer cells. In its place, manganese dioxide (MnO_2) NPs coated with a Hf-cisplatin-PEG shell showed a redox/pH/H_2O_2-responsive cancer treatment [85]. The NPs exhibited tumour activity wherein the oxygen level was elevated due to the presence of the MnO_2 core and displayed fast renal clearance. Moreover, a remarkable tumour growth inhibition was noticed after the combined chemoradiotherapy treatment without appreciable toxicity. In another example, Zhao *et al.* synthesised redox-sensitive mesoporous NCPs made of Mn(II) and dithiodiglycolic acid. The NPs encapsulated Dox and were protected with polydopamine (PDA) and PEG [152]. The disulfide linkage (SS) present in the dithiodiglycolic ligand was cleaved by GSH, leading to degradation of NCPs and Dox release (Fig. 16). Moreover, the NCPs demonstrated a concentration-dependent MRI contrast larger than clinically tested Gd CAs, providing efficient *in vivo* tumour accumulation. The NCPs exhibited good stability in the physiological environments and stable blood circulation after i.v. injection.

Yan *et col.* reported NCPs loaded with the photosensitive drug Ce6 using an amphiphilic amino-acid ligand coordinated with Mn(II) ions [153]. The NCPs showed significant drug loading capacity, high intrinsic biocompatibility, strong stability and PDT damage by releasing Ce6 upon coordination of GSH with Mn(II). Moreover, MRI was used to verify the antitumor efficacy *in vivo* (Fig. 17).

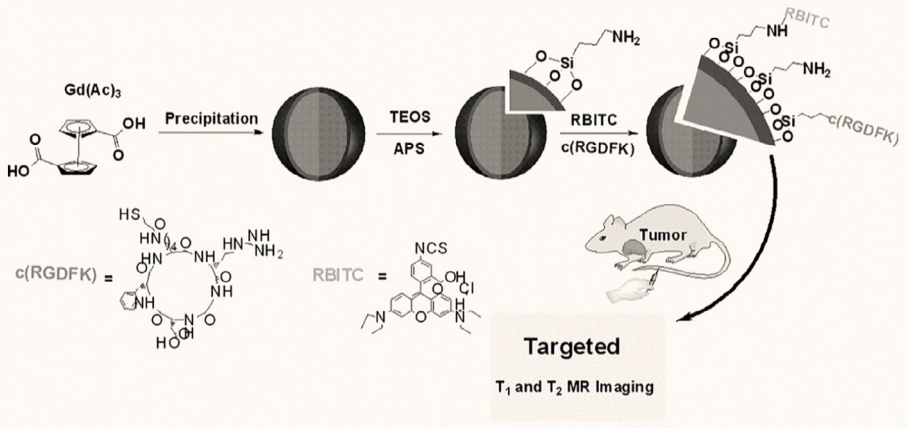

Fig. 15. Fc-Gd@SiO_2(RBITC)–RGD NCPs synthesis and their use as *in vivo* targeted dual-mode T_1- and T_2-weighted magnetic resonance imaging (MRI). Reproduced from Ref. [150] with permission of the copyright holder.

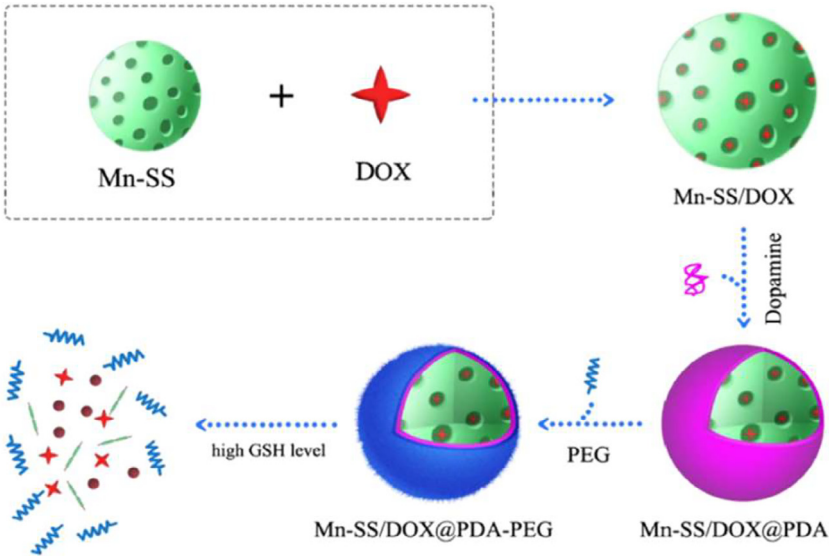

Fig. 16. Synthesis of Dox-loaded NCPs with glutathione (GSH)-triggered degradation. Reproduced from Ref. [152] with permission of the copyright holder.

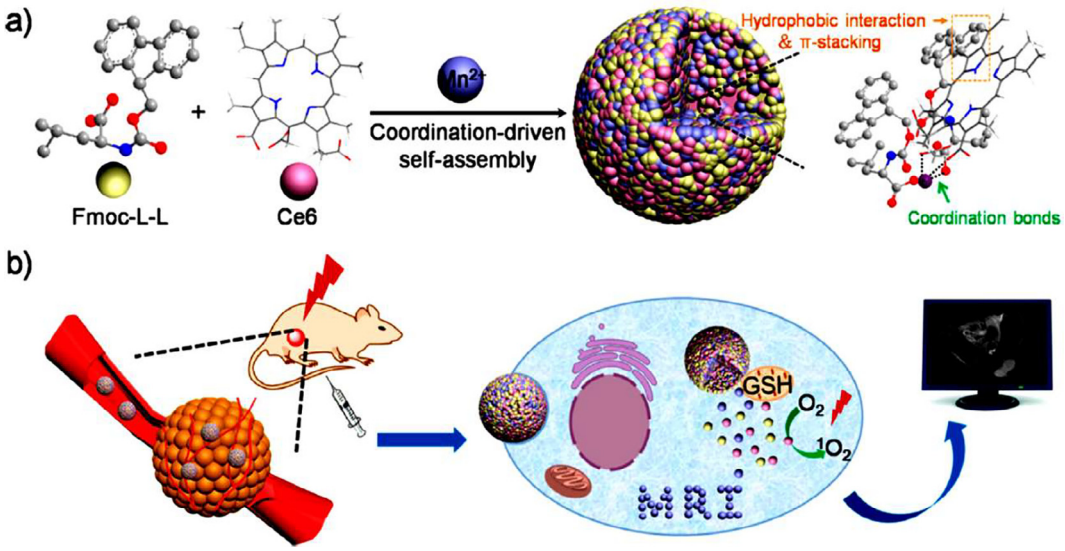

Fig. 17. Assembly and disassembly of FMCNPs for MRI-guided phtodynamic therapy (PDT). Reproduced from Ref. [153] with permission of the copyright holder.

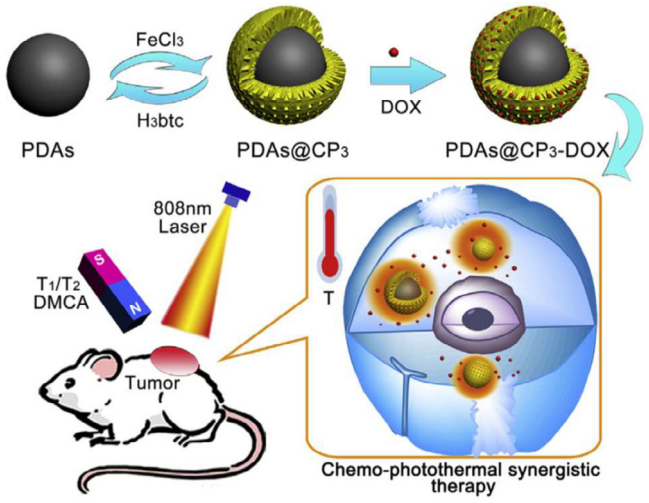

Fig. 18. Synthesis and application of PDAs@CP_3-Dox. Reproduced from Ref. [155] with permission of the copyright holder.

7.1.3. Iron-based NCPs

Zhao *et col.* described the synthesis of amphiphilic polymeric micelles encapsulating Dox and cross-linked through coordination bonds [154]. The presence of Fe(III) ions provided T_1-weighted (T_{1w}) MRI signals, while the acid-sensitive coordination bond of the drug allowed for its release and effective elimination of the 4T1 tumour in a mouse model. Lu *et col.* also developed PDA NPs with Fe ions for T_1/T_2 MRI and chemo-/photothermal therapy [155]. The *in vivo* performance of these NPs showed low toxicity and excellent biocompatibility. In addition, the chemotherapy was facilitated by delivering Dox on demand in response to NIR and by heat (Fig. 18). Following the efficient use of phenols, Mu *et col.* described the preparation of ultrasmall BSA-coated GA–Fe (III) NCPs that showed excellent biocompatibility and NIR absorption [156]. The NCPs provide good T_{1w} contrast as validated by *in vitro* and *in vivo* MRI experiments. *In vivo* intratumoural injection confirmed an antitumour activity combined with laser treatment (PTT) and monitored by the positive change in the MRI of the tumour.

Following a very successful approach, some of us reported NPs upon the reaction of a bis-imidazol (bix) ligand with different metal ions and phenol groups completing the coordination sphere. While the bis-imidazol ensures the polymerisation, the caffeic ligand confers: i) high robustness enforced by supramolecular hydrogen bonds without modifying the morphology and encapsulation abilities and ii) carboxylate groups located on at the surface of the NPs functionalised using peptide coupling reactions (Fig. 19). Moreover, these NPs exhibit high drug loading capacities, low cytotoxicity, efficient cell internalisation and control over the colloidal stability, becoming an excellent platform for their use as theranostic devices. The MRI properties of this novel platform were tested using three different metal ions (Fe(III), Gd(III) and Mn(II)), being the Fe-based NPs the ones showing enhanced *in vitro* phantoms and *ex vivo* dual-mode T_1/T_2 contrast [157].

In vivo MRI studies of the NPs in a murine glioblastoma model also showed a remarkable permanence for the simultaneous recording of T_1 values comparable to commercial CAs and an additional T_2 signal. Moreover, a subsequent gradual clearance denoted their good biodegradability Fig. 20 [157]. Beyond MRI, fluorescent multichannel imaging was also demonstrated. For this, fluorescein isothiocyanate (FITC), 1-pyrenebutanoic acid hydrazide (PBH) or Alexa Fluor® 568 (A568) were covalently linked to a catechol ligand. The NPs had good *in vitro* internalisation, retaining their characteristic fluorescence without significant dye leakage (Fig. 20) [158].

Finally, this platform was used to encapsulate different active materials taking advantage of its chemical flexibility. For instance, hybrid NCPs encapsulating superparamagnetic iron oxide NPs (SPIONs) acting as both T_1/T_2 CAs and efficient drug release systems were reported [159]. The NPs not only exhibited an efficient cellular uptake but a ten-fold efficacy versus the free drug in front of the human breast adenocarcinoma (MCF-7) cell line [33].

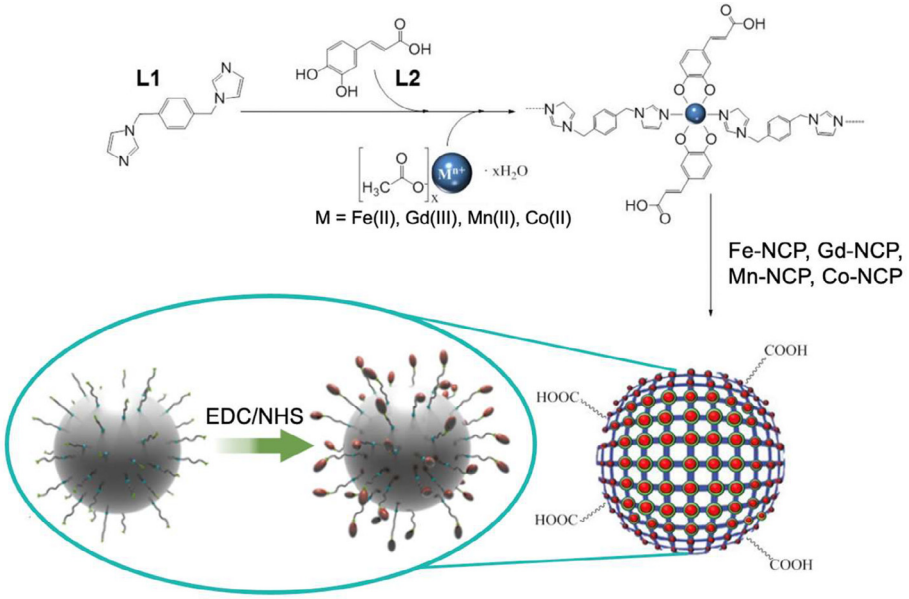

Fig. 19. Formation of NCPs based on bis-imidazol (L1, bix) and caffeic acid (L2) ligands. This approach allows for the fabrication of an extensive family of NCPs with different metal nodes, while carboxylates at the surface can be functionalised using peptide coupling reactions. Reproduced and adapted from Ref. [157] with permission of the copyright holder.

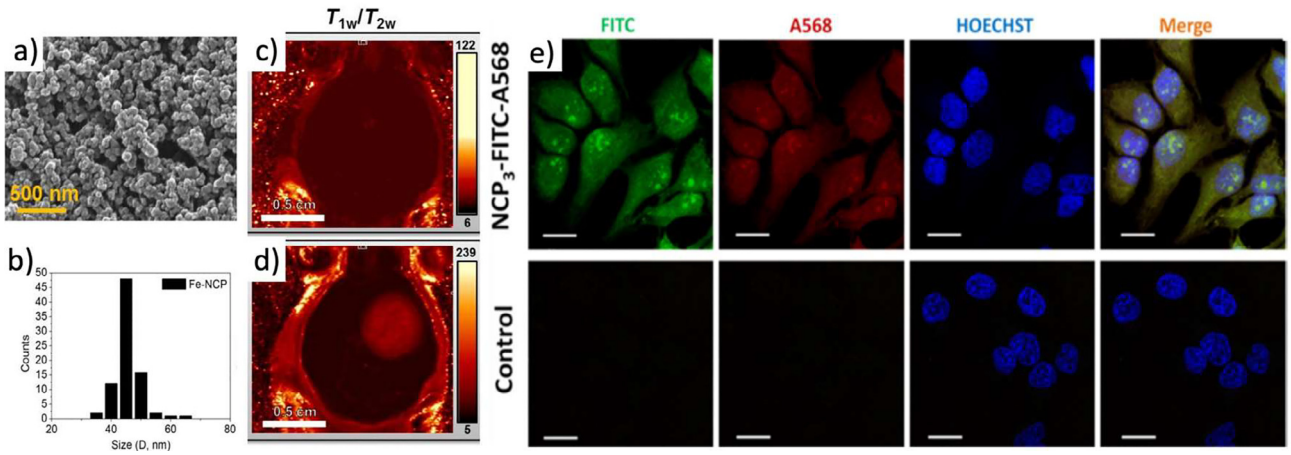

Fig. 20. a) SEM images; b) size histogram and *in vivo* T_{1w}/T_{2w} image; c) before and d) post i.v. injection of Fe-NCP; e) *in vivo* images using a confocal laser scanning microscopy of HeLa cells incubated with Co-NCP system for 2 h with NCP3-FITC-A568 (top) and the corresponding control (non-functionalised NCP). Different single-channel projections were displayed (FITC (green), A568 (red), the nuclear stain (Hoechst, blue)) and the merge of all the channels. Scale bars are 20 mm. Reproduced from Ref. [157] and [158] with permission of the copyright holder.

7.2. Other imaging/chemotherapy approaches

Fluorescent Zr-porphyrin NCPs loaded with Dox showed *in vivo* efficient accumulation in tumours combined with laser irradiation with residual side effects in healthy tissues [160]. In an additional example, Ban *et al.* synthesised amphiphilic hyperbranched polytriazoles containing Cu ions with aggregation-induced emission (AIE) enhancement used as a fluorescent probe [161]. The resulting nanocarrier was useful for cancer therapy in response to a redox stimulus that dissociated disulfide bonds and released the Cu complex units. As shown in other sections, radioimaging has also been used for the monitoring of NCPs. In this sense, Liu *et col.* reported renal-clearable NCPs coordinating W(VI) ions with PEG-functionalised GA and subsequently radiolabeled with ^{64}Cu for PET imaging (Fig. 21) [162]. The application of radiotherapy after the i.v. administration of the NCPs allowed for the inhibition of tumour growth. Interestingly, these NCPs showed very low *in vivo* toxicity and excellent clearance through the renal system.

Recently, we have described the modification of previously reported MRI-based NCPs [157] by adding In(III) and Cu(II) and their respective radioisotopes [163]. In this case, the PDA-like coating employed allowed for forming a functionalisable platform to incorporate PEG and folic acid for its specific targeting in CT26 tumour-bearing mice.

7.3. Multi-mode imaging/therapy approaches

7.3.1. MRI and optical imaging.

Yin *et col.* have developed NCPs using Gd(III) and Ru[4,4′-$(COOH)_2$bipyridyl(bpy)]$_3^{2+}$ with low toxicity and imaging ability

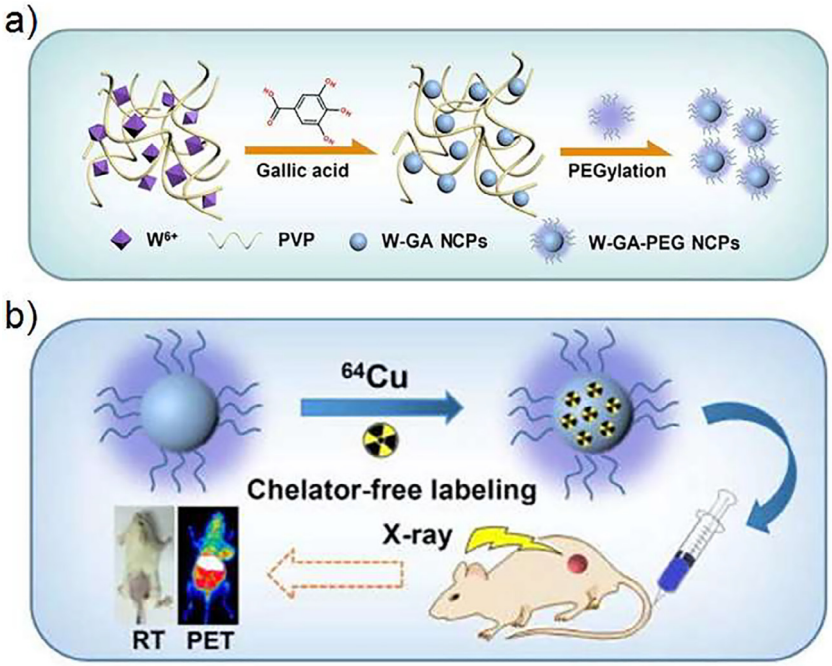

Fig. 21. a) synthesis W-GA-PEG NCPs and b) schematic of ^{64}Cu-labeled W-GA-PEG NCPs that enables positron emission tomography (PET) imaging and the radio-sensitising function of W(VI) for cancer radiotherapy. Reproduced from Ref. [162] with permission of the copyright holder.

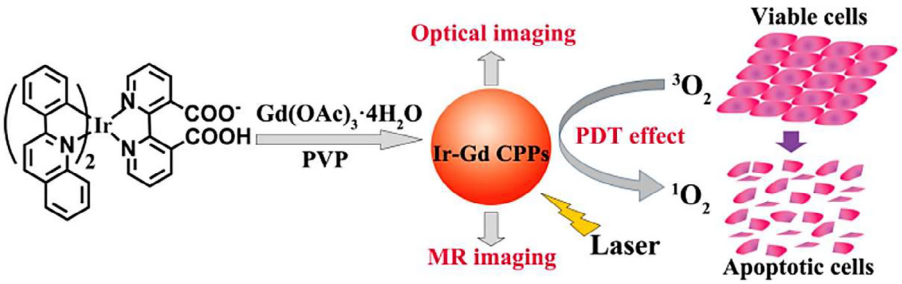

Fig. 22. Schematic synthesis and theranostic applications of Ir-Gd NCPs. Reproduced from Ref. [165] with permission of the copyright holder.

to differentiate tumours from other tissues thanks to a combination of high MRI contrast and red fluorescence emission [164]. In another example, Yang *et col.* stated stable and low toxicity NCPs with Ir(III) (luminescent) and magnetic Gd(III) ions (MRI probe) [165]. The NPs exhibited an efficient uptake by HeLa cells, while the efficient production of $^1O_2$ under visible irradiation allowed for PDT therapy of cancer cells (Fig. 22). Similarly, Yang *et al.* reported NCPs through the coordination between Mn(II) ions and IR825, a NIR dye, followed by PDA coating and PEGylation [166]. *In vivo* results demonstrated its efficacy as T_1 CA after gradual uptake by the tumour, high PTT efficacy and rapid renal excretion, minimising any long-term toxicity concern. Upon irradiation, tumours on mice with the NPs were entirely removed without reappearance in 60 days.

With a similar strategy, Qin *et al.* integrated diagnostic and therapeutic components into a single NCP. The ratio of coordinated Gd(III) and Fe(II) ions with polyphenols (i.e., TA) influenced the colloidal stability in an aqueous solution. These NPs revealed photothermal interconversion and longitudinal relaxivity that depended on the composition [167]. Those NPs (~23 nm) with a boosted Gd/Fe molar ratio exhibited an r_1 and r_2/r_1 ratio values of 9.3 mM^{-1} s^{-1} and 1.26, respectively, and high photothermal effectiveness. The *in vivo* assays in mice bearing EMT-6 tumours demonstrated the effective boost of tumour indicators and tumour growth suppression via PTT.

7.3.2. MRI and PAI.

Examples of NCPs systems able to give contrast in both MRI and PAI have been newly described. For example, Guo *et col.* designed a ground-breaking imaging agent combining an Fe_3O_4 nanocluster node and a carbocyanine-Gd(III) outer coating [168]. On top of that, folic acid-conjugated PEG chains were combined to improve the biodistribution and *in vivo* targeted delivery. Jin *et al.* reported ultra-small Fe-GA NCPs functionalised with PEG, displaying strong NIR absorbance, T_1 MR contrasting capability and high stability in various physiological environments [169]. Then, i.v. injection followed by photoacoustic tomography (PAT) and MRI bimodal imaging revealed tumour targeting without apparent toxicity. Interestingly, labelling with ^{64}Cu isotope also allowed for PET scanning. Finally, Hu *et al.* synthesised NCPs using PDA and Fe ions loaded with indocyanine green (ICG) for PAI/MRI and PTT cancer treatment [170]. ICG molecules increased remarkably the optical absorption of PDA NCPs in the NIR region and diminish their fluorescence emission, thus improving the PAI contrast and stimulating their photothermal conversion. Moreover, the Fe(III) ions coordinated with the PDA NCPs served for T_1 MRI. In a mouse 4T1 breast tumour model, these NCPs showed PAI/MRI dual-modal imaging and highly powerful PTT with noticeable therapeutic performance and minimum side effects.

7.3.3. Others

Yang *et al.* reported core–shell NCPs containing Mn(II) ions and IR825 dye for MRI and CT imaging, respectively, and Hf(IV) for CT and radio-sensitisation [171]. The NCPs were further coated with PDA and PEGylated, showing excellent eradication of tumours thanks to synergistic photothermal and radiation therapy in *in vivo* model experiments, without appreciable toxicity and efficient excretion. Liu *et col.* described Zn(II)-dipicolylamine NCPs loading ICG and therapeutic genes to accomplish a fluorescence/PAI-guided combination of phototherapy (PTT) and gene therapy [172]. In a 4T1 xenograft mouse model, PTT and gene therapy combined reduced the tumours with minimum side effects and, notably, without recurrence after three weeks. Finally, Yin *et col.* reported NCPs using $Ru[4,4'\text{-}(COOH)_2bpy]_3^{2+}$, Gd(III) and Yb(III) that allowed for red fluorescence, MRI and CT imaging with 3D spatial resolution and the $^1O_2$ production of the LRu for the efficient treatment of Hep G2 tumour-bearing mice [173]. Recently, G.-G. Yang *et al.* described the formation of NCPs through the coordination of quercetin (a heat shock protein inhibitor) with Fe(II) ions [174]. The NCPs showed specific accumulation in tumours due to the EPR effect. After the application of temperature, complete tumour ablation was achieved without damaging the surrounding healthy tissues. Additionally, these NCPs provided high resolution and depth tumour imaging, thanks to the combination of PAI and MRI. Worth to mention, this nanosystem presented high renal clearance ability, highlighting its safe clinical application and effectiveness for cancer treatment.

8. Perspectives and future trends

According to the excellent results reported over the last years, the use of NCPs with antitumoural activity can be considered in an embryonic development stage and still very promising. Most of the reported developments use metal chemotherapy and its combination with other active drugs (multifunctional nanodrugs) and/or CAs for imaging purposes (MRI, CT, SPECT/PET, and fluorescence, among others). All of this, along with new therapeutic developments such as PDT, PTT, or PA, allow us to predict that the blossom of these nanocarriers is yet to come. A schematic compilation of the most relevant anticancer NCPs revised is shown in Table 1, while Table 2 summarises NCPs combining diagnostic and therapeutic abilities. All-in-all, NCPs are strong prospective candidates to treat cancer thanks to their chemical versatility and the endless combination catalog available to mature novel nanomedicines with enhanced therapies. The interrogation that one poses then is: What steps are required from now on to achieve such an ambitious objective?

From our unassertive point of view, there are some main research areas that, in the short-medium term, deserve deep attention to successfully design the nanoplatforms of tomorrow if we want them to reach clinical phases. Those are described next:

- The first one is to devote more attention to the chemical composition of the NPs. In all examples reported, there is always a rational design but few delve into the exact chemical composi-

Table 1
Reported examples classified by the therapeutic activity of the NCPs.

Therapeutic modality	Active Metal	Metal Node	Ligand	Coating	Drug loaded	Cancer Type	Ref.
Metal chemotherapy	Pt	Zn(II)	DSP, 1,4-Bis(imidazol-1-ylmethyl)benzene	—	DSP	Breast, Cervix, Neuroblastoma	[43]
		Tb(III)	DSP	Silica coating	DSP	Colon	[55]
	Pt	Zn(II)	DSP	fatty acid-modified PEG	ALN	Breast	[56]
	Pt	Zr(IV), La(III)	DSP	Lipid coating	DSP	Lung	[95]
	Pt	Zn(II)	*Carboplatin-bis(phosphonic acid)*	Lipid coating	*Carboplatin-bis(phosphonic acid) prodrug + GcMP*	Ovarian	[96]
	Pt	Fe(III)	DSCP	cRGD functionalized PEG		Glioma	[97]
	Pt	Zn(II)	Bisphosphonic acids containing cisplatin and oxaliplatin prodrugs	Lipid coating	Cisplatin + oxaliplatin prodrugs	Pancreatic, Ovarian	[98,104,105]
	Pt	Zn(II)	Bisphosphonic acids containing oxaliplatin prodrug	Lipid coating	Oxaliplatin prodrug + GcMP	Pancreatic	[99]
	Pt	Zn(II)	*cis*,*cis*,*trans*-[$Pt(NH_3)_2Cl_2(OCONHP(O)(OH)_2)_2$],	pyropheophorbide-lipid conjugate	Cisplatin prodrug	Head and Neck	[100]
	Pt	Zn(II)	Pt(dach)(oxalate)(bisphosphoramidic acid)	Lipid coating	oxaliplatin prodrug + dihydroartemesinin (DHA)	Colorectal	[103]
	Pt	Zn(II)	$Pt^{IV}(en)_2$-bis(phosphonic acid)	PEG functionalized lipid bilayer	miRNA	Colorectal	[106]
	Pt	Fe(III)	Platinum prodrug polyphenols	PEG polyphenols	Cisplatin prodrug	Glioblastoma	[108]
	Pt	Gd(III)	Platinum prodrug polyphenols	block copolymers PEG-PDI-PDPA (PEG-PDI-C_{20})	Cisplatin prodrug	Glioblastoma	[109]
	Pt	Fe(III)	Platinum prodrug polyphenols	epigallocatechin-3-gallate (EGCG), polyphenol modified block copolymer (PEG-b-PPOH)	Cisplatin prodrug	Hepatic	[110]
	Cu	Cu(II)	2,20-bipyridyl, branched polyethyleneimine	—	—	Lung	[115]
	Cu	Cu(II)	Cu-3,5-bis(pyridin-3-ylmethylamino)benzoate	—	—	Cervix, Breast, Lung	[116]
	Cu	Cu(II)	1,10-phenanthroline and L-arginine	—	—	Breast	[117]
	Cu	Cu(II)	AQ4N + gossypol	hyaluronic acid	AQ4N + gossypol	Prostate	[118]
	Cu	Cu(II)	AQ4N, DOX		AQ4N + Dox + phthalocyanine	Hepatic	[119]
	Fe	Ru(II), Fe(II)	*bis(terpyridine) derivatives*	—	—	Lung	[121]
	Ru	Co(II)	2-oxo-1,2-dihydroquinoline-3-carbaldehyde (isonicotinic) hydrazine	—	—	Hepatic, Cervix, Skin	[122]
	Co	Co(II)	BPEI, dpq, ip	—	—	Breast	[123]
	Cu	Cu(II), Zn(II)	oxalic acid, *N*,*N*′-bis[2-(dimethylamino)ethyl]oxamide	—	—	—	[124]
	Co	As(III)	methoxy poly(ethylene oxide)-*block*-poly[α-(6-mecaptohexyl amino)carboxylate-ε-caprolactone] [PEO-*b*-P($CCLC_6$-SH)]	—	—	Breast	[126]
	As	La(III), Sr(II)	1,3,5-benzenetribenzoic acid (H_3BTB) and 4,4′,4″-(1,3,5-triazine-2,4,6-triyl)tribenzoic acid (H_3TATB)	—	—	Endometrial carcinoma	[127]
	La, Sr	In(III)	5-hydroxyisophthalic acid (H_3hip)	—	—	Lung	[128]
	In	Fe(II)	1,5-bis[(l-proline-1-yl)diazen-1-ium-1,2-diol-O^2-yl]-2,4-dinitrobenzene, [BPDB]	—	—	Hepatic	[132]
Non-Metal chemotherapy		Zn(II)	1,4-bis(imidazol-1-ylmethyl)benzene (bix)	—	Dox, SN-38, CPT, or DAU	Leukaemia	[44]
		Ca(II)	Pamidronate, Zoledronate	Lipid coating	Pamidronate, Zoledronate	Lung	[58,59]
		Cu(II)	PEG_{113}-$PBHE_m$-PS_n triblock copolymer	—	Dox	Cervix	[63]
Photodynamic therapy		Zn(II)	tetra(4-carboxyphenoxy)-phthalocyaninatozinc(II)	Lipid coating	—	Breast	[139]
		Ca(II)	AS1411 DNA G quadruplexes including Ce6 dye + hemin	—	—	Breast	[140]
		Zn(II)	porphyrin/G-quadruplex complexes and amphiphilic amino acids	anti-nucleolin aptamer (AS1411)		Cervical	[141]

Table 2
Use of reported NCPs as theranostic systems.

Imaging modality	Cancer Type	Metal	Ligands	Coating	Therapy	Ref.
MRI	Breast	MnO_2, Hf(IV)	DSP	Hf-DSP	Chemotherapy, radiotherapy	[85]
	Cervix	Gd(II)	pluronic F127 and a peptide-amphiphile	poly(ethylene-oxide) (PEO) + peptides	Chemotherapy	[149]
	Glioblastoma, Breast	Gd(II)	1,1′-dicarboxyl ferrocene (Fc)	rhodamine and RGD functionalized Silica coating	—	[150]
	Breast, Pancreatic	Mn(II)	Zoledronic acid	PEG-functionalized Lipid coating	Chemotherapy	[151]
	Breast, cervix, osteosarcoma	Mn(II)	dithiodiglycolic acid	PEGylated PDA	Chemotherapy	[152]
	Breast	Fe(III)	Catechol functionalized amphiphilic polymers	Polymeric coating	Chemotherapy	[154]
	Breast	Fe(III)	Gallic acid	BSA coating	PTT	[156]
	Glioblastoma	Fe(III), Gd(III), Mn (II)	Caffeic acid, 1,4-Bis(imidazol-1-ylmethyl)benzene	—	—	[157]
	Breast	Gd(III), Fe(III)	polyphenols	—	PTT	[167]
Dual-mode MRI	Cervix	Fe(III)	PDA	—	Chemotherapy, PTT	[155]
MIR/NIR	Cervix, Breast	Mn(II)	IR825 NIR dye	PEGylated PDA	PTT	[166]
MRI/Fluorescence	Breast	Mn(II)	amphiphilic amino-acid, Chlorin e6	—	PDT	[153]
	Hepatic	Gd(III)	$Ru[4,4'\text{-}(COOH)_2bipyridyl(bpy)]_3^{2+}$	—	—	[164]
MRI/ Phosphorescence	Cervix	Ir(II), Gd(III)	2-phenylquinoline; 3-carboxy-2,2′-bipyridyl-3′-carboxylate	polyvinylpyrrolidone (PVP)	—	[165]
MRI/PAI	Cervix	Fe_2O_4, Gd(III)	carbocyanine	Folic acid-conjugated PEG	—	[168]
	Breast	Fe(III)	Indocyanine green (ICG)–loaded polydopamine (PDA)	—	PTT	[170]
	Breast	Fe(II)	quercetin	—	Chemotherapy, PTT	[174]
MRI/PAI/PET	Breast, glioblastoma	Fe(III)	Gallic acid	PEG	PTT	[167]
MRI/Fluorescence/CT	Hepatic	Gd(III), Yb(III)	$Ru[4,4'\text{-}(COOH)_2bpy]_3^{2+}$	—	PDT	[173]
MRI/NIR/CT	Cervix, Breast	Mn(II), Hf(IV)	Mn/Hf-IR825	PEGylated PDA	PTT, Radiotherapy	[171]
Fluorescence/PAI	Breast	Zn(II)	dipicolylamine		PTT, gene therapy	[172]
Fluorescence	Hepatic	Zr(II)	Porphyrin	—	Chemotherapy, PDT	[160]
	Adenocarcinoma	Cu(II)	amphiphilic hyperbranched polytriazoles	—	Chemotherapy	[161]
PET	Breast	W(IV)	PEG functionalized gallic acid	—	Radiotherapy	[162]

tion. The difficulty is evident. Many of them are amorphous and without a well-defined chemical composition, as these NPs are obtained far from chemical equilibrium. Furthermore, many of them are obtained in a single reaction step together with lipid/polymeric coatings, targeting molecules, PEG, or other biomolecules. Thus, although a positive macroscopic effect can be identified in most cases, it is quite difficult (if not impossible) to establish a retroactive analysis that allows us to show an effective correlation between the real chemical composition versus the therapeutic effect.

- Second, several *in vivo* experiments have validated these NPs with: i) an excellent biodistribution with preferential retention in tumours mostly (EPR effect), ii) a suitable biodegradation profile that allows for the desired measurement and/or effects while avoiding toxic accumulation over long periods of time, iii) improvement of IC_{50} and image concerning free drugs and CAs and iv) the nanostructuration favours targeting and protection of the NPs while avoiding side effects. Therefore, further studies are required to understand and fine-tune the interaction of NCPs with the biological media and tissues, control the *in vivo* biodistribution kinetics, diffusion and degradation of the NPs, and control over the pharmacokinetics and efficiency of the carriers. Worth to mention, more effort is needed to efficiently study the different administration routes available to reach the tumor area efficiently. The most-reported administration route is i.v., which allows for a quick biodistribution through the bloodstream. Nevertheless, other administration routes are being exponentially tested, such as intranasally. In this last route, other aspects become relevant, for example, the mucoadhesion interaction with NCPs that could induce its retention, hampering its successful administration in the final location. The administration route could be selected depending on the type of tumour and its location. For example, brain-located tumours could be treated by administering NCPs via the intranasal pathway, avoiding crossing the blood-brain barrier. Each administration route has its advantages and disadvantages and its selection must be done accordingly to different issues: i) tumour location (e.g., brain, lungs, bladder), ii) NCPs features (e.g., size, stability, tissue interactions) and iii) side effects and toxicity.
- The variety of diseases and illnesses faced so far is very diverse. Perhaps the idea of concentrating ourselves in those where these systems have more potential would promote the area since there would be more synergism between different groups towards a common target.
- Finally, as far as we know, none of these systems is currently in the clinical phases. If the preclinical results are so interesting, why has translation not occurred yet? More rigorous testing is necessary to assess the clinical relevance and reproducibility when synthesised from different sources and following good manufacturing practice protocols. Moreover, additional commitments for the clinical implementation must be stretched, always in close collaboration with clinicians aware of the real needs of patients.

All-in-all, although there is still work ahead, the results obtained to date are very promising, especially considering that the blossom of these systems is relatively recent. In fact, the scientific community involved in this discipline grows exponentially every day, which allows us to face these new challenges with a very positive attitude of success in the medium-long term.

Declaration of Competing Interest

The authors declare that they have no known competing financial interests or personal relationships that could have appeared to influence the work reported in this paper.

Acknowledgments

This work was supported by grants RTI2018-098027-B-C21, PID2019-106403RB-I00 and RED2018-102471-T from the Spanish Government funds and by the European Regional Development Fund (ERDF). The ICN2 is funded by the CERCA programme/Generalitat de Catalunya. The ICN2 is supported by the Severo Ochoa Centres of Excellence programme, funded by the Spanish Research Agency (AEI, grant no. SEV-2017-0706). R. S. thanks the Ministerio de Educación, Cultura y Deporte for the predoctoral grant FPU14/03170. S.S.-G. acknowledges the support from MINECO BES-2015-071492 grant. Special thanks to Dr. Javier Saiz-Poseu from 3D Science Visuals (Instagram: 3dscivisuals) for contributing with graphic design and scientific illustrations.

References

[1] R.K. Jain, T. Stylianopoulos, Delivering nanomedicine to solid tumors, Nat. Rev. Clin. Oncol. 7 (2010) 653–664.
[2] R.K. Jain, Delivery of molecular and cellular medicine to solid tumors, Adv. Drug Deliv. Rev. 64 (2012) 353–365.
[3] I. Brigger, C. Dubernet, P. Couvreur, Nanoparticles in cancer therapy and diagnosis, Adv. Drug. Deliv. Rev. 64 (2012) 24–36.
[4] S.D. Steichen, M. Caldorera-Moore, N. Peppas, A review of current nanoparticle and targeting moieties for the delivery of cancer therapeutics, Eur. J. Pharm. Sci. 48 (2013) 416–427.
[5] S.R. D'Mello, C.N. Cruz, M.L. Chen, K.M. Tyner, The evolving landscape of drug products containing nanomaterials in the United States, Nat. Nanotechnol. 12 (2017) 523–529.
[6] P. Evers, Nanotechnology in Medical Applications: The Global Market, BCC Research (Business Communications Company (BCC) Inc., Wellesley, MA, USA, 2017.
[7] R.A. Petros, J.M. Desimone, Strategies in the design of nanoparticles for therapeutic applications, Nat. Rev. Drug Discovery 9 (2010) 615–627.
[8] C.L. Ventola, Progress in nanomedicine: approved and investigational nanodrugs. P&T: a Peer-reviewed, J. Formul. Manage. 42 (2017) 742–755.
[9] T.M. Allen, P.R. Cullis, Liposomal drug delivery systems: From concept to clinical applications, Adv. Drug Deliv. Rev. 65 (2013) 36–48.
[10] S.E. Lohse, C.J. Murphy, Applications of colloidal inorganic nanoparticles: from medicine to energy, J. Am. Chem. Soc. 134 (2012) 15607–15620.
[11] M. Arruebo, Drug delivery from structured porous inorganic materials, Wiley Interdiscip. Rev. Nanobiotechnology 4 (2012) 16–30.
[12] D. Peer, J.M. Karp, S. Hong, O.C. Farokhzad, R. Margalit, R. Langer, Nanocarriers as an emerging platform for cancer therapy, Nature Nanotech. 2 (2007) 751–760.
[13] A. Baeza, D. Ruiz-Molina, M. Vallet-Regí, Expert Opin. Drug Deliv. 14 (2017) 783–796.
[14] M. Kim, H. Na, Y. Kim, S.R. Ryoo, H.S. Cho, K.E. Lee, H. Jeon, R. Ryoo, D.H. Min, Facile synthesis of monodispersed mesoporous silica nanoparticles with ultralarge pores and their application in gene delivery, ACS Nano 5 (2011) 3568–3576.
[15] L. Yuan, Z. Yanli, C. Xiaoyuan, Bioengineering of metal-organic frameworks for nanomedicine, Theranostics 9 (2019) 3122–3133.
[16] P. Horcajada, C. Serre, M. Vallet-Regí, M. Sebban, F. Taulelle, G. Férey, Metal–organic frameworks as efficient materials for drug delivery, Angew. Chem. 118 (2006) 6120–6124.
[17] R. Anand, F. Borghi, F. Manoli, I. Manet, V. Agostoni, P. Reschiglian, R. Gref, S. Monti, Host-guest interactions in Fe(III)-trimesate MOF nanoparticles loaded with doxorubicin, J. Phys. Chem. B 118 (2014) 8532–8539.
[18] M. Giménez-Marqués, T. Hidalgo, C. Serre, P. Horcajada, Nanostructured metal–organic frameworks and their bio-related applications, Coord. Chem. Rev. 307 (2015) 1–19.
[19] C. Wen, J. Wang, C. Chengchao, C. Wei, W. Chunsheng, L. Gang, Metal-organic framework-based stimuli-responsive systems for drug delivery, Adv. Sci. 6 (2019) 1801526.
[20] L. Wang, M. Zheng, Z. Xie, Nanoscale metal–organic frameworks for drug delivery: a conventional platform with new promise, J. Mater. Chem. B 6 (2018) 707–717.
[21] K. Böll, A. Zimpel, O. Dietrich, S. Wuttke, M. Peller, Clinically approved MRI contrast agents as imaging labels for a porous iron-based MOF nanocarrier: a systematic investigation in a clinical MRI setting, Adv. Ther. 3 (2020) 1900126.
[22] M. Oh, C.A. Mirkin, Chemically tailorable colloidal particles from infinite coordination polymers, Nature 438 (2005) 651–654.
[23] X. Sun, S. Dong, E. Wang, Coordination-induced formation of submicrometer-scale, monodisperse, spherical colloids of organic-inorganic hybrid materials at room temperature, J. Am. Chem. Soc. 127 (2005) 13102–13103.
[24] J. Puigmartí-Luis, Microfluidic platforms: A mainstream technology for the preparation of crystals, Chem. Soc. Rev. 43 (2014) 2253–2271.

[25] M. Guardingo, P. González-Monje, F. Novio, E. Bellido, F. Busqué, G. Molnár, A. Bousseksou, D. Ruiz-Molina, Synthesis of nanoscale coordination polymers in femtoliter reactors on surfaces, ACS Nano 10 (2016) 3206–3213.
[26] E. Bellido, P. González-Monje, M. Guardingo, F. Novio, A. Sánchez, M. Montero, G. Molnar, A. Bousseksou, D. Ruiz-Molina, Nanoscale coordination polymers obtained in ultrasmall liquid droplets on solid surfaces and its comparison to different synthetic volume scales, RSC Adv. 6 (2016) 76666–76672.
[27] M. Guardingo, F. Busqué, D. Ruiz-Molina, Reactions in ultra-small droplets by tip-assisted chemistry, Chem. Commun. 52 (2016) 11617–11626.
[28] A. Bousseksou, G. Molnár, L. Salmon, W. Nicolazzi, Molecular spin crossover phenomenon: recent achievements and prospects, Chem. Soc. Rev. 40 (2011) 3313–3335.
[29] I. Imaz, D. Maspoch, C. Rodríguez-Blanco, J.M. Pérez-Falcón, J. Campo, D. Ruiz-Molina, Valence-tautomeric metal-organic nanoparticles, Angew. Chem. Int. Ed. 47 (2008) 1857–1860.
[30] F. Novio, J. Simmchen, N. Vázquez-Mera, L. Amorín-Ferré, D. Ruiz-Molina, Coordination polymer nanoparticles in medicine, Coord. Chem. Rev. 257 (2013) 2839–2847.
[31] K.M.L. Taylor-Pashow, J. Della Rocca, Z. Xie, S. Tran, W. Lin, Postsynthetic modifications of iron-carboxylate nanoscale metal–organic frameworks for imaging and drug delivery, J. Am. Chem. Soc. 131 (2009) 14261–14263.
[32] S.M. Cohen, Postsynthetic methods for the functionalization of metal-organic frameworks, Chem. Rev. 112 (2012) 970–1000.
[33] F. Novio, J. Lorenzo, F. Nador, K. Wnuk, D. Ruiz-Molina, Carboxyl group (-CO2H) functionalized coordination polymer nanoparticles as efficient platforms for drug delivery, Chem. Eur. J. 20 (2014) 15443–15450.
[34] F. Novio, D. Ruiz-Molina, Hydrophobic coordination polymer nanoparticles and application for oil–water separation, RSC Adv. 4 (2014) 15293–15296.
[35] P. Gonzalez-Monje, F. Novio, D. Ruiz-Molina, Covalent grafting of coordination polymers on surfaces: the case of hybrid valence tautomeric interphases, Chem. Eur. J. 21 (2015) 10094–10099.
[36] Y. Bi, F. Hao, G. Yan, L. Teng, R.J. Lee, J. Xie, Actively targeted nanoparticles for drug delivery to tumor, Curr. Drug Metab. 17 (2016) 763–782.
[37] J. Duan, W. Jin, S. Kitagawa, Water-resistant porus coordination polymers for gas separation, Coord. Chem. Rev. 332 (2017) 48–74.
[38] Y.-B. Huang, Q. Wang, J. Liang, X. Wang, R. Cao, Soluble metal-nanoaprticle-decorated porous coordination polymers for the homogenization of heterogeneous catalysis, J. Am. Chem. Soc. 138 (2016) 10104–10107.
[39] J. Deng, F. Wu, P. Yu, L. Mao, On-site sensors based on infinite coordination polymer nanoaprticles: Recent progress and future challenge, Appl. Mater. Today 11 (2018) 338–351.
[40] E.S. Sebastian, A. Rodríguez-Diéguez, J.M. Seco, J. Cepeda, Coordination polymers with intriguing photoluminescence beahavior: The promising avenue for greatest long-lasting phosphors, Eur. J. Inorg. Chem. 2018 (2018) 2155–2174.
[41] J.-S.M. Lee, K. Otake, S. Kitagawa, Transport properties in porous coordination polymers, Coord. Chem. Rev. 421 (2020) 213447.
[42] I. Imaz, J. Hernando, D. Ruiz-Molina, D. Maspoch, Metal-organic spheres as functional systems for guest encapsulation, Angew. Chem. Int. Ed. 48 (2009) 2325–2329.
[43] N.N. Adarsh, C. Frias, T.M. Ponnoth Lohidakshan, J. Lorenzo, F. Novio, J. Garcia-Pardo, D. Ruiz-Molina, Pt(IV)-based nanoscale coordination polymers: Antitumor activity, cellular uptake and interactions with nuclear DNA, Chem. Eng. J. 340 (2018) 94–102.
[44] L. Amorín-Ferré, F. Busqué, J.L. Bourdelande, D. Ruiz-Molina, J. Hernando, F. Novio, Encapsulation and release mechanisms in coordination polymer nanoparticles, Chem. Eur. J. 19 (2013) 17508–17516.
[45] I. Imaz, M. Rubio-Martínez, L. García-Fernández, F. García, D. Ruiz-Molina, J. Hernando, V. Puntes, D. Maspoch, Coordination polymer particles as potential drug delivery systems, Chem. Commun. 46 (2010) 4737–4739.
[46] P.F. Gao, L.L. Zheng, L.J. Liang, X.X. Yang, Y.F. Li, C.Z. Huang, A new type of pH-responsive coordination polymer sphere as a vehicle for targeted anticancer drug delivery and sustained release, J. Mater. Chem. B 1 (2013) 3202–3208.
[47] G. Liang, H. Ni, S. Bao, F. Zhu, H. Gao, Q. Wu, Synthesis and characterization of nanowire coils of organometallic coordination polymers for controlled cargo release, J. Phys. Chem. B 118 (2014) 6339–6345.
[48] C. Fan, D.A. Wang, Novel gelatin-based nano-gels with coordination-induced drug loading for intracellular delivery, J. Mater. Sci. Technol. 32 (2016) 840–844.
[49] L. Xing, Y. Cao, S. Che, Synthesis of core–shell coordination polymer nanoparticles (NCPs) for pH-responsive controlled drug release, Chem. Commun. 48 (2012) 5995–5997.
[50] R.C. Huxford, K.E. deKrafft, W.S. Boyle, D. Liu, W. Lin, Lipid-coated nanoscale coordination polymers for targeted delivery of antifolates to cancer cells, Chem. Sci. 3 (2012) 198–204.
[51] X. Yan, Y. Li, Q. Zou, C. Yuan, S. Li, R. Xing, Amino acid coordination-driven self-assembly for enhancing both biological stability and tumor accumulation of curcumin, Angew. Chem. Int. Ed. 57 (2018) 17084–17088.
[52] M. Li, C. Wang, Z. Di, H. Li, J. Zhang, W. Xue, M. Zhao, K. Zhang, Y. Zhao, L. Li, Engineering multifunctional DNA hybrid nanospheres through coordination-driven self-assembly, Angew. Chem. Int. Ed. 58 (2019) 1350–1354.
[53] Z. Fan, L. Sun, Y. Huang, Y. Wang, M. Zhang, Bioinspired fluorescent dipeptide nanoparticles for targeted cancer cell imaging and real-time monitoring of drug release, Nat. Nanotechnol. 11 (2016) 388–394.
[54] N. Bertleff-Zieschang, M.A. Rahim, Y. Ju, J.A. Braunger, T. Suma, Y. Dai, S. Pan, F. Cavalieri, F. Caruso, Biofunctional metal-phenolic films from dietary flavonoids, Chem. Commun. 53 (2017) 1068–1071.
[55] W.J. Rieter, K.M. Pott, K.M.L. Taylor, W. Lin, Nanoscale coordination polymers for platinum-based anticancer drug delivery, J. Am. Chem. Soc. 130 (2008) 11584–11585.
[56] H. Yuanfeng, H. Yanjuan, H. Ziyuan, Y. Jiang, X. Sun, Y. Shen, W. Chu, C. Zhao, Bisphosphonate-functionalized coordination polymer nanoparticles for the treatment of bone metastatic breast cancer, J. Control. Release 264 (2017) 76–88.
[57] J.R. Green, Bisphosphonates: preclinical review, Oncologist 9 (2004) 3–13.
[58] S. Wang, J. Della Rocca, W. Lin, R.C. Huxford-Phillips, S.A. Kramer, D. Liu, Coercing bisphosphonates to kill cancer cells with nanoscale coordination polymers, Chem. Commun. 48 (2012) 2668–2670.
[59] E. Alvarez, A.G. Marquez, T. Devic, N. Steunou, C. Serre, C. Bonhomme, C. Gervais, I. Izquierdo-Barba, M. Vallet-Regi, D. Laurencin, F. Mauri, P. Horcajada, A biocompatible calcium bisphosphonate coordination polymer: towards a metal-linker synergistic therapeutic effect?, CrystEngComm 15 (2013) 9899–9905.
[60] R. Solórzano, O. Tort, J. García-Pardo, T. Escribà, J. Lorenzo, M. Arnedo, D. Ruiz-Molina, R. Alibés, F. Busqué, F. Novio, Biomater. Sci. 7 (2019) 178–186.
[61] K. Han, W.Y. Zhang, J. Zhang, Z.Y. Ma, H.Y. Han, pH-responsive nanoscale coordination polymer for efficient drug delivery and real-time release monitoring, Adv. Healthc. Mater. 6 (2017) 1–9.
[62] S. Xu, J. Liu, D. Li, L. Wang, J. Guo, C. Wang, C. Chen, Fe-Salphen complexes from intracellular pH-triggered degradation Of Fe3O4@Salphen-InIII CPPs for selectively killing cancer cells, Biomaterials 35 (2014) 1676–1685.
[63] L. Bai, F. Song, X.H. Wang, J.Y.Q. Cao, X. Han, X.L. Wang, Y.Z. Wang, Ligand-metal-drug coordination based micelles for efficient intracellular doxorubicin delivery, RSC Adv. 5 (2015) 47629–47639.
[64] B. Wang, M. Jacquet, K. Wang, K. Xiong, M. Yan, J. Courtois, G. Royal, pH-induced fragmentation of colloids based on responsive self-assembled copper (II) metallopolymers, New J. Chem. 42 (2018) 7823–7829.
[65] T. Wang, X. Liu, Y. Zhu, Z.D. Cui, X.J. Yang, H. Pan, K.W.K. Yeung, S. Wu, Metal ion coordination polymer-capped pH-triggered drug release system on titania nanotubes for enhancing self-antibacterial capability of Ti Implants, ACS Biomater. Sci. Eng. 3 (2017) 816–825.
[66] W. Huang, P. Hao, J. Qin, S. Luo, T. Zhang, B. Peng, H. Chen, X. Zan, Hexahistidine-metal assemblies: a promising drug delivery system, Acta Biomater. 90 (2019) 441–452.
[67] Y. Yang, L. Xu, W. Zhu, L. Feng, J. Liu, Q. Chen, Z. Dong, J. Zhao, Z. Liu, M. Chen, One-pot synthesis of pH-responsive charge-switchable PEGylated nanoscale coordination polymers for improved cancer therapy, Biomaterials 156 (2018) 121–133.
[68] H. Ejima, J.J. Richardson, K. Liang, J.P. Best, M.P. Van Koeverden, G.K. Such, J. Cui, F. Caruso, One-step assembly of coordination complexes for versatile film and particle engineering, Science 341 (2013) 154–157.
[69] M.A. Rahim, H. Ejima, K.L. Cho, K. Kempe, M. Müllner, J.P. Best, F. Caruso, Coordination-driven multistep assembly of metal-polyphenol films and capsules, Chem. Mater. 26 (2014) 1645–1653.
[70] Y. Ping, J. Guo, H. Ejima, X. Chen, J.J. Richardson, H. Sun, F. Caruso, pH-responsive capsules engineered from metal-phenolic networks for anticancer drug delivery, Small 11 (2015) 2032–2036.
[71] J. Li, C. Zhang, S. Gong, X. Li, M. Yu, C. Qian, H. Qiao, M. Sun, A nanoscale photothermal agent based on a metal-organic coordination polymer as a drug-loading framework for effective combination therapy, Acta Biomater. 94 (2019) 435–446.
[72] Y. Ju, J. Cui, H. Sun, M. Müllner, Y. Dai, J. Guo, N. Bertleff-Zieschang, T. Suma, J. J. Richardson, F. Caruso, Engineered metal-phenolic capsules show tunable targeted delivery to cancer cells, Biomacromolecules 17 (2016) 2268–2276.
[73] Y. Ju, Q. Dai, J. Cui, Y. Dai, T. Suma, J.J. Richardson, F. Caruso, Improving targeting of metal-phenolic capsules by the presence of protein coronas, ACS Appl. Mater. Interfaces 8 (2016) 22914–22922.
[74] J.H. Park, K. Kim, J. Lee, J.Y. Choi, D. Hong, S.H. Yang, F. Caruso, Y. Lee, I.S. Choi, A cytoprotective and degradable metal-polyphenol nanoshell for single-cell encapsulation, Angew. Chem. Int. Ed. 53 (2014) 12420–12425.
[75] Q.Q. Besford, Y. Ju, T.Y. Wang, G. Yun, P.V. Cherepanov, C.E. Hagemeyer, F. Cavalieri, F. Caruso, Self-assembled metal-phenolic networks on emulsions as low-fouling and pH-responsive particles, Small 14 (2018) 1–9.
[76] J. Liu, H. Wang, X. Yi, Y. Chao, Y. Geng, L. Xu, K. Yang, Z. Liu, pH-sensitive dissociable nanoscale coordination polymers with drug loading for synergistically enhanced chemoradiotherapy, Adv. Funct. Mater. 27 (2017) 1–10.
[77] J. Liu, L. Tian, R. Zhang, Z. Dong, H. Wang, Z. Liu, Collagenase-encapsulated pH-responsive nanoscale coordination polymers for tumor microenvironment modulation and enhanced photodynamic nanomedicine, ACS Appl. Mater. Interfaces 10 (2018) 43493–43502.
[78] F. Nador, F. Novio, D. Ruiz-Molina, Coordination polymer particles with ligand-centred pH-responses and spin transition, Chem. Commun. 50 (2014) 14570–14572.
[79] Y. Zhang, Y. Guo, S. Wu, H. Liang, H. Xu, Photodegradable coordination polymer particles for light-controlled cargo release, ACS Omega 2 (2017) 2536–2543.
[80] J. Liu, G. Yang, W. Zhu, Z. Dong, Y. Yang, Y. Chao, Z. Liu, Light-controlled drug release from singlet-oxygen sensitive nanoscale coordination polymers enabling cancer combination therapy, Biomaterials 146 (2017) 40–48.

[81] X.G. Hu, X. Li, S.I. Yang, Novel photochromic infinite coordination polymer particles derived from a diarylethene photoswitch, Chem. Commun. 51 (2015) 10636–10639.
[82] P.V. Cherepanov, M.A. Rahim, N. Bertleff-Zieschang, M.A. Sayeed, A.P. O'Mullane, S.E. Moulton, F. Caruso, Electrochemical behavior and redox-dependent disassembly of gallic acid/FeIIIMetal-phenolic networks, ACS Appl. Mater. Interfaces 10 (2018) 5828–5834.
[83] S. Buwalda, B. Nottelet, A. Bethry, R.J. Kok, N. Sijbrandi, J. Coudane, Reversibly core-crosslinked PEG-P(HPMA) micelles: platinum coordination chemistry for competitive-ligand-regulated drug delivery, J. Colloid Interface Sci. 535 (2019) 505–515.
[84] S. Li, Q. Zou, Y. Li, C. Yuan, R. Xing, X. Yan, Smart peptide-based supramolecular photodynamic metallo-nanodrugs designed by multicomponent coordination self-assembly, J. Am. Chem. Soc. 140 (2018) 10794–10802.
[85] J. Liu, Q. Chen, W. Zhu, X. Yi, Y. Yang, Z. Dong, Z. Liu, Nanoscale-coordination-polymer-shelled manganese dioxide composite nanoparticles: A multistage redox/pH/H2O2-responsive cancer theranostic nanoplatform, Adv. Funct. Mater. 27 (2017) 1605926.
[86] Y. Wang, Y. Wu, F. Li, D. Chen, Folic acid-modified iridium(III) coordination polymeric nanoparticles facilitating intracellular release of a phosphorescent residue capable of nuclear entry, Inorg. Chem. Commun. 40 (2014) 143–147.
[87] F. Pu, E. Ju, J. Ren, X. Qu, Multiconfigurable logic gates based on fluorescence switching in adaptive coordination polymer nanoparticles, Adv. Mater. 26 (2014) 1111–1117.
[88] F. Pu, J. Ren, X. Qu, "Plug and Play" logic gates based on fluorescence switching regulated by self-assembly of nucleotide and lanthanide ions, ACS Appl. Mater. Interfaces 6 (2014) 9557–9562.
[89] R.-R. Gao, S. Shi, Y.-J. Li, M. Wumaier, X.-C. Hu, T.-M. Yao, Coordination polymer nanoparticles from nucleotide and lanthanide ions as a versatile platform for color-tunable luminescence and integrating boolean logic operations, Nanoscale 9 (2017) 9589–9597.
[90] L. Bai, X.H. Wang, F. Song, X.L. Wang, Y.Z. Wang, "AND" Logic gate regulated pH and reduction dual-responsive prodrug nanoparticles for efficient intracellular anticancer drug delivery, Chem. Commun. 51 (2015) 93–96.
[91] L. Kelland, The resurgence of platinum-based cancer chemotherapy, Nat. Rev. Cancer 7 (2007) 573–584.
[92] T.C. Johnstone, K. Suntharalingam, S.J. Lippard, The next generation of platinum drugs: targeted Pt(II) agents, nanoparticle delivery, and Pt(IV) prodrugs, Chem. Rev. 116 (2016) 3436–3486.
[93] X. Duan, C. He, S.J. Kron, W. Lin, Nanoparticle formulations of cisplatin for cancer therapy, WIREs Nanomed. Nanobiotechnol. 8 (2016) 776–791.
[94] N. Graf, T.E. MokhtariLoannis, A. Papayannopoulos, S.J. Lippard, Platinum(IV)-chlorotoxin (CTX) conjugates for targeting cancer cells, J. Inorg. Biochem. 110 (2012) 58–63.
[95] R.C. Huxford-Phillips, S.R. Russell, D. Liu, W. Lin, Lipid-coated nanoscale coordination polymers for targeted cisplatin delivery, RSC Adv. 3 (2013) 14438–14443.
[96] C. Poon, X. Duan, C. Chan, W. Han, W. Lin, Nanoscale coordination polymers codeliver carboplatin and gemcitabine for highly effective treatment of platinum-resistant ovarian cancer, Mol. Pharm. 13 (2016) 3665–3675.
[97] J. Liu, M. Wu, Y. Pan, Y. Duan, Z. Dong, Y. Chao, Z. Liu, B. Liu, Biodegradable nanoscale coordination polymers for targeted tumor combination therapy with oxidative stress amplification, Adv. Funct. Mater. 30 (2020) 1908865.
[98] D. Liu, C. Poon, K. Lu, C. He, W. Lin, Self-assembled nanoscale coordination polymers with trigger release properties for effective anticancer therapy, Nat. Commun. 5 (2014) 4182.
[99] C. Poon, C. He, D. Liu, K. Lu, W. Lin, Self-assembled nanoscale coordination polymers carrying oxaliplatin and gemcitabine for synergistic combination therapy of pancreatic cancer, J. Control. Release 201 (2015) 90–99.
[100] C. He, D. Liu, W. Lin, Self-assembled core-shell nanoparticles for combined chemotherapy and photodynamic therapy of resistant head and neck cancers, ACS Nano 9 (2015) 991–1003.
[101] P. Velpurisiva, A. Gad, B. Piel, R. Jadia, P. Rai, Nanoparticle design strategies for effective cancer immunotherapy, J. Biomed. 2 (2017) 64–77.
[102] C. He, X. Duan, N. Guo, C. Chan, C. Poon, R.R. Weichselbaum, W. Lin, Core-shell nanoscale coordination polymers combine chemotherapy and photodynamic therapy to potentiate checkpoint blockade cancer immunotherapy, Nat. Commun. 7 (2016) 1–12.
[103] X. Duan, C. Chan, W. Han, N. Guo, R.R. Weichselbaum, W. Lin, Immunostimulatory nanomedicines synergize with checkpoint blockade immunotherapy to eradicate colorectal tumors, Nat. Commun. 10 (2019) 1899.
[104] C. He, D. Liu, W. Lin, Self-assembled nanoscale coordination polymers carrying SiRNAs and cisplatin for effective treatment of resistant ovarian cancer, Biomaterials 36 (2015) 124–133.
[105] C. He, C. Poon, C. Chan, S.D. Yamada, W. Lin, Nanoscale coordination polymers codeliver chemotherapeutics and siRNAs to eradicate tumors of cisplatin-resistant ovarian cancer, J. Am. Chem. Soc. 138 (2016) 6010–6019.
[106] C. Chan, N. Guo, X. Duan, W. Han, L. Xue, D. Bryan, S.C. Wightman, N.N. Khodarev, R.R. Weichselbaum, W. Lin, Systemic MiRNA delivery by nontoxic nanoscale coordination polymers limits epithelial-to-mesenchymal transition and suppresses liver metastases of colorectal cancer, Biomaterials 210 (2019) 94–104.
[107] Y. Dai, J. Guo, T.-Y. Wang, Y. Ju, A.J. Mitchell, Th. Bonnard, J. Cui, J.J. Richardson, Ch.E. Hagemeyer, K. Alt, F. Caruso, Self-Assembled nanoparticles from phenolic derivatives for cancer therapy, Adv. Healthc. Mater. 6 (2017) 1700467.
[108] Y. Dai, S. Cheng, Zh. Wang, R. Zhang, Z. Yang, J. Wang, B.C. Yung, Z. Wang, O. Jacobson, C. Xu, Q. Ni, G. Yu, Z. Zhou, X. Chen, Hypochlorous acid promoted platinum drug chemotherapy by myeloperoxidase-encapsulated therapeutic metal phenolic nanoparticles, ACS Nano 12 (2018) 455–464.
[109] Z. Yang, Y. Dai, L. Shan, Z. Shen, Z. Wang, B.C. Yung, O. Jacobson, Y. Liu, W. Tang, S. Wang, L. Lin, G. Niu, P. Huang, X. Chen, Tumor microenvironment-responsive semiconducting polymer-based self-assembling nanotheranostics, Nanoscale Horiz. 4 (2019) 426–433.
[110] Z. Ren, S. Sun, R. Sun, G. Cui, L. Hong, B. Rao, A. Li, Z. Yu, Q. Kan, Z. Mao, A metal–polyphenol-coordinated nanomedicine for synergistic cascade cancer chemotherapy and chemodynamic therapy, Adv. Mater. 32 (2020) 1906024.
[111] U. Ndagi, N. Mhlongo, M.E. Soliman, Metal complexes in cancer therapy – an update from drug design perspective, Drug Des. Devel. Ther. 11 (2017) 599–616.
[112] A. Bindoli, M.P. Rigobello, G. Scutari, C. Gabbiani, A. Casini, L. Messori, Thioredoxin reductase: a target for gold compounds acting as potential anticancer drugs, Coord. Chem. Rev. 253 (2009) 1692–1707.
[113] I. Kostova, Ruthenium complexes as anticancer agents, Curr. Med. Chem. 13 (2006) 1085–1107.
[114] P.C. Bruijnincx, P.J. Sadler, New trends for metal complexes with anticancer activity, Curr. Opin. Chem. Biol. 12 (2008) 197–206.
[115] R.S.Kumar,V.S.Periasamy,C.P.Paul,A.Riyasdeen,S.Arunachalam,M.A.Akbarsha, Cytotoxic effect of a polymer-copper(II) complex containing 2,20-bipyridyl ligand on human lung cancer cells, Med. Chem. Res. 20 (2011) 726–731.
[116] K. Wang, X. Ma, D. Shao, Z. Geng, Z. Zhang, Z. Wang, Coordination-induced assembly of coordination polymer submicrospheres: promising antibacterial and in vitro anticancer activities, Cryst. Growth Des. 12 (2012) 3786–3791.
[117] J. Lakshmipraba, S. Arunachalam, A. Riyasdeen, R. Dhivya, S. Vignesh, M.A. Akbarsha, R.A. James, DNA/RNA binding and anticancer/antimicrobial activities of polymer-copper(II) complexes, Spectrochim. Acta - Part A Mol. Biomol. Spectrosc. 109 (2013) 23–31.
[118] S. Shen, Y. Wu, K. Li, Y. Wang, J. Wu, Y. Zeng, D. Wu, Versatile hyaluronic acid modified AQ4N-Cu(II)-gossypol infinite coordination polymer nanoparticles: multiple tumor targeting highly efficient synergistic chemotherapy, and real-time self-monitoring, Biomaterials 154 (2018) 197–212.
[119] D. Zhang, M. Wu, Z. Cai, N. Liao, K. Ke, H. Liu, M. Li, G. Liu, H. Yang, X. Liu, J. Liu, Chemotherapeutic drug based metal-organic particles for microvesicle-mediated deep penetration and programmable pH/NIR/hypoxia activated cancer photochemotherapy, Adv. Sci. 5 (2018) 1700648.
[120] L. Zeng, P. Gupta, Y. Chen, E. Wang, L. Ji, H. Chao, Z.S. Chen, The development of anticancer ruthenium(II) complexes: from single molecule compounds to nanomaterials, Chem. Soc. Rev. 46 (2017) 5771–5804.
[121] J. Li, T. Murakami, M. Higuchi, Metallo-supramolecular polymers: versatile DNA binding and their cytotoxicity, J. Inorg. Organomet. Polym. Mater. 23 (2013) 119–125.
[122] D.S. Raja, N.S.P. Bhuvanesh, K. Natarajan, Novel water soluble ligand bridged cobalt(II) coordination polymer of 2-oxo-1,2-dihydroquinoline-3-carbaldehyde (isonicotinic) hydrazone: evaluation of the DNA binding, protein interaction, radical scavenging and anticancer activity, Dalton Trans. 41 (2012) 4365–4377.
[123] S. Nehru, S. Arunachalam, R. Arun, K. Premkumar, Polymer-Cobalt(III) complexes: structural analysis of metal chelates on DNA interaction and comparative cytotoxic activity, J. Biomol. Struct. Dyn. 32 (2014) 1876–1888.
[124] M. Jiang, Y.T. Li, Z.Y. Synthesis, Structure, cytotoxic activities, and DNA-binding of 1-D copper(II) and Zinc(II) coordination polymers, J. Coord. Chem. 65 (2012) 1858–1871.
[125] C.E. Carraher, M.R. Roner, N. Pham, A. Moric-Johnson, Group VA polyesters containing thiodiglycolic acid-synthesis and preliminary cancer activity, J. Macromol. Sci. Part A Pure Appl. Chem. 51 (2014) 547–556.
[126] Q. Zhang, M.R. Vakili, X.F. Li, A. Lavasanifar, X.C. Le, Polymeric micelles for GSH-triggered delivery of arsenic species to cancer cells, Biomaterials 35 (2014) 7088–7100.
[127] Y. Wang, L. Duan, X. Luo, Q. Deng, J. Xie, J. Jin, K. Zhang, Two new metal coordination polymers: anticancer activity in endometrial carcinoma, Inorg. Nano-Metal Chem. 48 (2018) 257–261.
[128] D. Shu, W. Chen, Synthesis, structure, and in vitro anti-lung cancer activity on an in-based nanoscale coordination polymer, Main Group Met. Chem. 41 (2018) 129–133.
[129] L.A. Ostrovskaya, L.V. Zhilitskaya, K.A. Abzaeva, D.B. Korman, V.A. Rikova, M. M. Fomina, M.G. Voronkov, N.V. Bluhterova, Polyacrylates of noble metals as potential antitumor drugs, Biophysics (Oxf) 59 (2014) 642–645.
[130] I. Romero-Canelón, P.J. Sadler, Next-generation metal anticancer complexes: multitargeting via redox modulation, Inorg. Chem. 52 (2013) 12276–12291.
[131] Y. Geldmacher, M. Oleszak, W.S. Sheldrick, Rhodium(III) and iridium(III) complexes as anticancer agents, Inorg. Chim. Acta 393 (2012) 84–102.
[132] Y. Hu, T. Lv, Y. Ma, J. Xu, Y. Zhang, Y. Hou, Z. Huang, Y. Ding, Nanoscale coordination polymers for synergistic NO and chemodynamic therapy of liver cancer, Nano Lett. 19 (2019) 2731–2738.
[133] P. Agostinis, K. Berg, K.A. Cengel, T.H. Foster, A.W. Girotti, S.O. Gollnick, S.M. Hahn, M.R. Hamblin, A. Juzeniene, D. Kessel, M. Korbelik, J. Moan, P. Mroz, D.

Nowis, J. Piette, B.C. Wilson, J. Golab, Photodynamic therapy of cancer: an update, CA Cancer J. Clin. 61 (2017) 250–281.
[134] K. Lu, C. He, W. Lin, Nanoscale metal-organic framework for highly effective photodynamic therapy of resistant head and neck cancer, J. Am. Chem. Soc. 136 (2014) 16712–16715.
[135] Q. Guan, Y.A. Li, W.Y. Li, Y.B. Dong, Photodynamic therapy based on nanoscale metal-organic frameworks: from material design to cancer nanotherapeutics, Chem. Asian J. 13 (2018) 3122–3149.
[136] R. Chen, J. Zhang, J. Chelora, Y. Xiong, S.V. Kershaw, K.F. Li, P.K. Lo, K.W. Cheah, A.L. Rogach, J.A. Zapien, C.-S. Lee, Ruthenium(II) complex incorporated UiO-67 metal-organic framework nanoparticles for enhanced two-photon fluorescence imaging and photodynamic cancer therapy, ACS Appl. Mater. Interfaces 9 (2017) 5699–5708.
[137] K. Lu, C. He, W. Lin, A chlorin-based nanoscale metal-organic framework for photodynamic therapy of colon cancers, J. Am. Chem. Soc. 137 (2015) 7600–7603.
[138] L.P. Roguin, N. Chiarante, M.C. García Vior, J. Marino, Zinc(II) phthalocyanines as photosensitizers for antitumor photodynamic therapy, Int. J. Biochem. Cell Biol. 114 (2019) 105575.
[139] Z. Huang, L. Huang, Y. Huang, Y. He, X. Sun, X. Fu, X. Xu, G. Wei, D. Chen, C. Zhao, Phthalocyanine-based coordination polymer nanoparticles for enhanced photodynamic therapy, Nanoscale 9 (2017) 15883–15894.
[140] Y. Yang, W. Zhu, L. Feng, Y. Chao, X. Yi, Z. Dong, K. Yang, W. Tan, Z. Liu, M. Chen, G-quadruplex-based nanoscale coordination polymers to modulate tumor hypoxia and achieve nuclear-targeted drug delivery for enhanced photodynamic therapy, Nano Lett. 18 (2018) 6867–6875.
[141] J.-Q. Chu, D.-X. Wang, L.-M. Zhang, M. Cheng, R.-Z. Gao, C.-G. Gu, P.-F. Lang, P.-Q. Liu, L.-N. Zhu, D.-M. Kong, Green layer-by-layer assembly of porphyrin/G-quadruplex-based near-infrared nanocomposite photosensitizer with high biocompatibility and bioavailability, ACS Appl. Mater. Interfaces 12 (2020) 7575–7585.
[142] X. Wang, J. Liang, C. Zhang, G. Ma, C. Wang, D. Kong, Coordination microparticle vaccines engineered from tumor cell templates, Chem. Commun. 55 (2019) 1568–1571.
[143] C.M. Calabrese, T.J. Merkel, W.E. Briley, P.S. Randeria, S.P. Narayan, J.L. Rouge, D.A. Walker, A.W. Scott, C.A. Mirkin, Biocompatible infinite-coordination-polymer nanoparticle-nucleic-acid conjugates for antisense gene regulation, Angew. Chem. Int. Ed. 54 (2015) 476–480.
[144] Y. Chao, C. Liang, Y. Yang, G. Wang, D. Maiti, L. Tian, F. Wang, W. Pan, S. Wu, K. Yang, Z. Liu, Highly effective radioisotope cancer therapy with a non-therapeutic isotope delivered and sensitized by nanoscale coordination polymers, ACS Nano 12 (2018) 7519–7528.
[145] Q. Yang, Z. Zhou, L. Cui, H. Yang, C. Yan, X. Zhou, S. Yang, L. Pan, X. Zhang, Coordination polymer hybridized au nanocages: a nanoplatform for dual-modality imaging guided near-infrared driven photothermal therapy in vivo, J. Mater. Chem. B 5 (2017) 8761–8769.
[146] S. Suárez-García, R. Solórzano, F. Novio, R. Alibés, F. Busqué, D. Ruiz-Molina, Coordination polymers nanoaprticles for bioimaging, Coord. Chem. Rev. 432 (2021) 213716.
[147] E.-K. Lim, T. Kim, S. Paik, Nanomaterials for theranostics: recent advances and future challenges, Reviews 115 (2015) 327–394.
[148] Z. He, P. Zhang, Y. Xiao, J. Li, F. Yang, Y. Liu, J.R. Zhang, J.J. Zhu, Acid-degradable gadolinium-based nanoscale coordination polymer: a potential platform for targeted drug delivery and potential magnetic resonance imaging, Nano Res. 11 (2018) 929–939.
[149] J. Ma, H. Dong, H. Zhu, C.W. Li, Y. Li, D. Shi, Deposition of gadolinium onto the shell structure of micelles for integrated magnetic resonance imaging and robust drug delivery systems, J. Mater. Chem. B 4 (2016) 6094–6102.
[150] H. Yang, C. Qin, C. Yu, Y. Lu, H. Zhang, F. Xue, D. Wu, Z. Zhou, S. Yang, RGD-conjugated nanoscale coordination polymers for targeted T1- and T2-weighted magnetic resonance imaging of tumors in vivo, Adv. Funct. Mater. 24 (2014) 1738–1747.
[151] D. Liu, C. He, C. Poon, W. Lin, Theranostic nanoscale coordination polymers for magnetic resonance imaging and bisphosphonate delivery, J. Mater. Chem. B 2 (2014) 8249–8255.
[152] J. Zhao, Y. Yang, X. Han, C. Liang, J. Liu, X. Song, Z. Ge, Z. Liu, Redox-sensitive nanoscale coordination polymers for drug delivery and cancer theranostics, ACS Appl. Mater. Interfaces 9 (2017) 23555–23563.
[153] H. Zhang, K. Liu, S. Li, X. Xin, S. Yuan, G. Ma, X. Yan, Self-assembled minimalist multifunctional theranostic nanoplatform for magnetic resonance imaging-guided tumor photodynamic therapy, ACS Nano 12 (2018) 8266–8276.
[154] K. Xin, M. Li, D. Lu, X. Meng, J. Deng, D. Kong, D. Ding, Z. Wang, Y. Zhao, Bioinspired coordination micelles integrating high stability, triggered cargo release, and magnetic resonance imaging, ACS Appl. Mater. Interfaces 9 (2017) 80–91.
[155] Y. Chen, K. Ai, J. Liu, X. Ren, C. Jiang, L. Lu, Polydopamine-based coordination nanocomplex for T1/T2 dual mode magnetic resonance imaging-guided chemo-photothermal synergistic therapy, Biomaterials 77 (2016) 198–206.
[156] X. Mu, C. Yan, Q. Tian, J. Lin, S. Yang, BSA-assisted synthesis of ultrasmall gallic acid-Fe(III) coordination polymer nanoparticles for cancer theranostics, Int. J. Nanomed. 12 (2017) 7207–7223.
[157] S. Suárez-García, N. Arias-Ramos, C. Frias, A.P. Candiota, C. Arús, J. Lorenzo, D. Ruiz-Molina, F. Novio, Dual T1/T2 nanoscale coordination polymers as novel contrast agents for MRI: A preclinical study for brain tumor, ACS Appl. Mater. Interfaces 10 (2018) 38819–38832.
[158] F. Nador, K. Wnuk, J. García-Pardo, J. Lorenzo, R. Solorzano, D. Ruiz-Molina, F. Novio, Dual-fluorescent nanoscale coordination polymers via a mixed-ligand synthetic strategy and their use for multichannel imaging, ChemNanoMat 4 (2018) 183–193.
[159] M. Borges, S. Yu, A. Laromaine, A. Roig, S. Suárez-García, J. Lorenzo, D. Ruiz-Molina, F. Novio, Dual T1/T2 MRI contrast agent based on hybrid SPION@coordination polymer nanoparticle, RSC Adv. 5 (2015) 86779–86783.
[160] W. Liu, Y.M. Wang, Y.H. Li, S.J. Cai, X.B. Yin, X.W. He, Y.K. Zhang, Fluorescent imaging-guided chemotherapy-and-photodynamic dual therapy with nanoscale porphyrin metal-organic framework, Small 13 (2017) 1–8.
[161] Q. Ban, J. Du, W. Sun, J. Chen, S. Wu, J. Kong, Intramolecular copper-containing hyperbranched polytriazole assemblies for label-free cellular bioimaging and redox-triggered copper complex delivery, Macromol. Rapid Commun. 39 (2018) 1800171.
[162] S. Shen, D. Jiang, L. Cheng, Y. Chao, K. Nie, Z. Dong, C.J. Kutyreff, J.W. Engle, P. Huang, W. Cai, et al., Renal-clearable ultrasmall coordination polymer nanodots for chelator-free 64Cu-labeling and imaging-guided enhanced radiotherapy of cancer, ACS Nano 11 (2017) 9103–9111.
[163] S. Suárez-García, T.V.F. Esposito, J. Neufeld-Peters, M. Bergamo, H. Yang, K. Saatchi, P. Schaffer, U.O. Häfeli, D. Ruiz-Molina, C. Rodríguez-Rodríguez, F. Novio, Hybrid metal-phenol nanoaprticles with polydopamine like coating for PET/SPECT/CT imaging, ACS Appl. Mater. Interfaces 13 (2021) 10705–10718.
[164] Y.M. Wang, W. Liu, X.B. Yin, Self-limiting growth nanoscale coordination polymers for fluorescence and magnetic resonance dual-modality imaging, Adv. Funct. Mater. 26 (2016) 8463–8470.
[165] Y. Lu, F. Xue, H. Yang, M. Shi, Y. Yan, L. Qin, Z. Zhou, S. Yang, Phosphorescent coordination polymer nanoparticles as a three-in-one platform for optical imaging, T1-weighted magnetic resonance imaging, and photodynamic therapy, J. Phys. Chem. C 119 (2015) 573–579.
[166] Y. Yang, J. Liu, C. Liang, L. Feng, T. Fu, Z. Dong, Y. Chao, Y. Li, G. Lu, M. Chen, Z. Liu, Nanoscale metal-organic particles with rapid clearance for magnetic resonance imaging-guided photothermal therapy, ACS Nano 10 (2016) 2774–2781.
[167] J. Qin, G. Liang, Y. Feng, B. Feng, G. Wang, N. Wu, Y. Zhao, J. Wei, Synthesis of gadolinium/iron–bimetal–phenolic coordination polymer nanoparticles for theranostic applications, Nanoscale 12 (2020) 6096–6103.
[168] Q. An, J. Liu, M. Yu, J. Wan, D. Li, C. Wang, C. Chen, J. Guo, Multifunctional magnetic Gd3+-based coordination polymer nanoparticles: combination of magnetic resonance and multispectral optoacoustic detections for tumor-targeted imaging in vivo, Small 11 (2015) 5675–5686.
[169] Q. Jin, W. Zhu, D. Jiang, R. Zhang, C.J. Kutyreff, J.W. Engle, P. Huang, W. Cai, Z. Liu, L. Cheng, Ultra-small iron-gallic acid coordination polymer nanoparticles for chelator-free labeling of 64Cu and multimodal imaging-guided photothermal therapy, Nanoscale 9 (2017) 12609–12617.
[170] D. Hu, C. Liu, L. Song, H. Cui, G. Gao, P. Liu, Z. Sheng, L. Cai, Indocyanine green-loaded polydopamine-iron ions coordination nanoparticles for photoacoustic/magnetic resonance dual-modal imaging-guided cancer photothermal therapy, Nanoscale 8 (2016) 17150–17158.
[171] Y. Yang, Y. Chao, J. Liu, Z. Dong, W. He, R. Zhang, K. Yang, M. Chen, Z. Liu, Core-shell and co-doped nanoscale metal-organic particles (NMOPs) obtained via post-synthesis cation exchange for multimodal imaging and synergistic thermo-radiotherapy, NPG Asia Mater. 9 (2017) e344.
[172] C. Chu, E. Ren, Y. Zhang, J. Yu, H. Lin, X. Pang, Y. Zhang, H. Liu, Z. Qin, Y. Cheng, X. Wang, W. Li, X. Kong, X. Chen, G. Liu, Zinc(II)-dipicolylamine coordination nanotheranostics: toward synergistic nanomedicine by combined photo/gene therapy, Angew. Chem. Int. Ed. 58 (2019) 269–272.
[173] Y.M. Wang, W. Liu, X.B. Yin, Multifunctional mixed-metal nanoscale coordination polymers for triple-modality imaging-guided photodynamic therapy, Chem. Sci. 8 (2017) 3891–3897.
[174] G.-G. Yang, D.-J. Zhou, Z.-Y. Pan, J. Yang, D.-Y. Zhang, Q. Cao, L.-N. Ji, Z.-W. Mao, Multifunctional low-temperature photothermal nanodrug with in vivo clearance, ROS-Scavenging and anti-inflammatory abilities, Biomaterials 216 (2019) 119280.
[176] N. N. Adarsh, F. Novio, D. Ruiz-Molina, Coordination Polymers Built from 1,4-Bis(Imidazol-1-Ylmethyl)Benzene: From Crystalline to Amorphous, Dalton Transactions 45 (2016) 11233–11255.